Title: Vascular transcription factors guide plant epidermal responses to limiting phosphate conditions

Authors: Jos R. Wendrich[1,2,†], BaoJun Yang[1,2,†], Niels Vandamme[3,4,†], Kevin Verstaen[3,4,†], Wouter Smet[1,2], Celien Van de Velde[1,2], Max Minne[1,2], Brecht Wybouw[1,2], Eliana Mor[1,2], Helena E. Arents[1,2], Jonah Nolf[1,2], Julie Van Duyse[5,6], Gert Van Isterdael[5,6], Steven Maere[1,2], Yvan Saeys[3,4,*] and Bert De Rybel[1,2,*]

Affiliations:

[1] Ghent University, Department of Plant Biotechnology and Bioinformatics, Ghent, Belgium

[2] VIB Center for Plant Systems Biology, Ghent, Belgium

[3] Data Mining and Modelling for Biomedicine, VIB Center for Inflammation Research, Ghent, Belgium

[4] Ghent University, Department of Applied Mathematics, Computer Science and Statistics, Ghent, Belgium

[5] VIB Flow Core, VIB Center for Inflammation Research, Ghent, Belgium

[6] Ghent University, Department of Biomedical Molecular Biology, Ghent, Belgium

[†] equal contribution

* Correspondence to: Bert De Rybel (beryb@psb.vib-ugent.be) and Yvan Saeys (yvan.saeys@irc.vib-ugent.be)

Abstract:

Optimal plant growth is hampered by deficiency of the essential macronutrient phosphate in most soils. Plant roots can however increase their root hair density to efficiently forage the soil for this immobile nutrient. By generating and exploiting a high-resolution single-cell gene expression atlas of Arabidopsis roots, we show an enrichment of TARGET OF MONOPTEROS 5 / LONESOME HIGHWAY (TMO5/LHW) target gene responses in root hair cells. The TMO5/LHW heterodimer triggers biosynthesis of mobile cytokinin in vascular cells and increases root hair density during low phosphate conditions by modifying both the length and cell fate of epidermal cells. Moreover, root hair responses in phosphate deprived conditions are TMO5 and cytokinin dependent. In conclusion, cytokinin signaling links root hair responses in the epidermis to perception of phosphate depletion in vascular cells.

Main Text:

Vascular cell proliferation in plant roots is, in part, controlled by the heterodimer complex formed by TARGET OF MONOPTEROS 5 and LONESOME HIGHWAY (TMO5/LHW) (*1-7*). This complex is required and sufficient to control cell proliferation by inducing expression of the direct downstream target *LONELY GUY4* (*LOG4*) and its close homolog *LOG3* (*1, 6*), which encode rate-limiting enzymes in the final conversion step of the phytohormone cytokinin into its bio-active form (*8, 9*). The TMO5/LHW complex is limited to xylem cells, which produce cytokinin but are themselves insensitive to cytokinin. The xylem-produced cytokinin diffuses to neighboring procambium cells, where it promotes cell proliferation via induction of DOF-type transcription factors (*10, 11*). As the TMO5/LHW pathway induces production of cytokinin as mobile intermediate that functions in neighboring cells, the target genes (*11*) in this hormone signaling cascade are likely to be expressed in various cell types surrounding the xylem and perhaps even outside of the vascular bundle. Here we used single cell RNA-sequencing to probe the tissue specific TMO5/LHW signaling output in Arabidopsis root meristems and found that this vascular heterodimer complex is required for the root hair responses to phosphate deficit conditions. We show how cytokinin signaling links vascular perception of limiting phosphate to epidermal responses allowing plants to efficiently forage the soil for this immobile macronutrient.

Single cell RNA-sequencing analysis

We generated a high-resolution single cell RNA-sequencing (scRNA-seq) atlas of the wild type Arabidopsis root tip (*12-16*), making use of the 10X Genomics Chromium technology (**Fig. S1A**). Following protoplast isolation, sorted cells were collected and processed for single cell transcriptomics (see Supplementary Materials for details). In summary, a total population of 15,918 cells were recovered across three replicates and next filtered to retain 5,145 high quality cells with unique molecular identifier (UMI) counts > 17,290 (**Fig. S1B**). Taking into account only these high quality cells, a total of 21,492 genes were detected in our root meristem dataset, covering nearly 80% of the genome, with a median expression of 6,781 genes per cell and a mean of 208,937 reads per cell (**Fig. 1A**). Unsupervised clustering and *t*-distributed stochastic neighbor-embedding (tSNE) projections were performed on the 5,145 high quality single cells, recovering distinct clusters of cells (**Fig. 1A**).

Following quality control (see Supplementary Materials and **Fig. S1C-E**), cell type annotation and cluster identification were performed by mapping the top 20 differentially expressed genes (DEG) for each cluster (compared to the rest of the dataset) on a publicly available bulk RNA-seq dataset (*17*) of the Arabidopsis root. This resulted in an annotated dataset representing all major cell types in the root, including quiescent center cells (**Fig. 1A, S1F**). The annotations were confirmed for all cell identities by the observed expression of key signature marker genes and *in vivo* expression of 41 newly generated promoter reporter lines (**Fig. 1B, S2-12** and **Table S1**). Moreover, cells undergoing division are found in two specific sub-clusters (**Fig. 1**), indicating that their transcriptomes are more similar to each other than the actual cell identity determinants of the transcriptome. In summary, the scRNA-seq dataset contains clusters of all cell types of the root meristem which were identified according to predicted *in vivo* expression patterns and were validated using a set of newly generated reporter lines.

Trajectory analysis establishes a blueprint of cell lineages

We next used trajectory analyses to refine identification of cell types and developmental transitions within each cell identity cluster. We first analyzed xylem (251 cells; 5%; **Fig. S3A**) and phloem (388 cells; 8%; **Fig. S4A**) cell lineages, as these undergo identity changes throughout development. Xylem initial cell lineages branch into proto- and metaxylem identities, which differ in their subsequent differentiation processes including secondary cell wall generation (*18*). Phloem cell initials undergo several oriented divisions, generating lineages that branch to generate phloem procambium, sieve elements and companion cells (*19, 20*). The complexity of both these cell types was captured in the inferred trajectories and gene expression patterns of the reporter lines validated inferred developmental trajectories and sub-cluster identities (**Fig. S3** and **S4**; see Supplementary Materials for details). Similar analyses validated trajectories for the procambium, pericycle, endodermis, cortex, epidermis, lateral root cap and columella clusters (**Fig. 1A** and **S5-S11**).

As many root cell types in Arabidopsis increase in ploidy with development (*21*), the developmental trajectories for these cell types should correspond to trajectories of increasing cellular endoreplication levels. Thus, to further validate our trajectories, we predicted the endoreplication state of each cell based on the expression of a validated set of endoreplication markers (*21*) (see Supplementary Materials for details) and superimposed the predicted cell ploidy on the tSNE plot (**Fig. 1C**). Developmental trajectories of cortex, endodermis, pericycle, epidermis/atrichoblast, lateral root cap and xylem clusters exhibit clear ploidy transitions (**Fig. 1C**); validating these trajectories and their orientation. For the procambium cell cluster, correspondence between developmental trajectories and ploidy was less evident. For the phloem cell lineage, which undergoes continuous divisions as it passes through the meristem, no correlation was found. Cells in the quiescent center and hair cell (trichoblast) clusters mostly contained 2C and 16C cells, respectively (**Fig. 1C**).

In conclusion, both newly generated reporter lines and ploidy analysis confirm the inferred developmental trajectories of all main cell identities. Our results thus allow the identification of distinct sub-clusters linked to the developmental stage of each cell identity; establishing a developmental blueprint for all root cell lineages, including progenitor populations for several cell identities.

TMO5/LHW targets are enriched in root hair cells

We next intersected our scRNA-seq root dataset with the set of 273 genes identified via bulk transcriptome analysis to be induced upon TMO5/LHW induction (*11*). About 80 target genes (29%) were predicted to be expressed in root hair (trichoblast) cells, of which 47 (17%) were expressed only in trichoblast cells (**Fig. 2A** and **S13**). Such expression patterns were not expected in relation to literature on TMO5/LHW function in vascular proliferation (*1, 2, 5, 6*) and the overlapping expression domain in the young xylem cells (*2*). We confirmed the induction and expression pattern of a subset of these genes by Q-RT-PCR and promoter-GFP fusions respectively (**Fig**. **2B** and **S14A**). The trichoblast specific expression patterns of these target genes thus suggests a putative role for TMO5/LHW in the regulation of root hair development or patterning. Although homozygous *tmo5* single and *tmo5 tmo5-like1* double mutants showed normal root hair densities under standard growth conditions (high phosphate, HP), misexpression of *TMO5* and *LHW* in all cells of the root meristem (p*RPS5A*::TMO5-GR x p*RPS5A*::LHW-GR or dGR) resulted in a strong increase in root hair density (**Fig. 2C-D**); while misexpression of

unrelated bHLH factors did not result in this root hair density increase (**Fig. S15**). A strong increase in root hair density can also be observed in wild type roots grown on phosphate limiting conditions (**Fig. 2C-D** and **Table S2**; see **Fig. S16** and Supplementary Materials for a detailed description of 3D root hair quantifications) (*22-24*). Auxin biosynthesis, transport and signaling are all required for this root hair response to phosphate limiting conditions (*22*): auxin signaling is induced upon low phosphate conditions in the columella/lateral root cap region and in xylem cells, where the TMO5/LHW dimer is active (*2, 4*). Auxin-dependent TMO5 function is required for the root hair response to low phosphate, as *tmo5 tmo5-like1* double mutants were less sensitive to these limiting conditions (**Fig. 2C-D** and **Table S2**). Phosphate starvation genes (*25*) were however still induced in this mutant background (**Fig. S14B**), suggesting that perception was unaffected. Moreover, induction of several root hair specific TMO5/LHW target genes was *tmo5 tmo5-like1* dependent (**Fig. S14C**). The TMO5 homologs seem redundantly required for this response, as we found no significant difference in root hair density between wild type and the *tmo5* single mutant on low phosphate (**Fig. 2C-D**) (*26*). Taken together, these results show that the increase in root hair density upon low phosphate conditions specifically requires TMO5 activity. Because low phosphate conditions have also been associated with changes in root hair length (*27*), we quantified this parameter in our mutant lines and treatments and found similar responses (**Fig. S14D**; see **Fig. S16** and Supplementary Materials for details on quantification**)**. Thus, activity of the TMO5/LHW complex is required for the complete root hair response to low phosphate conditions.

To understand the cellular basis of the root hair density increase in response to low phosphate conditions, we quantified several parameters that could contribute to this effect (including root length, meristem length and epidermal cell length; **Fig. 2E**, **S14E-F** and **S16**) in wild type and *tmo5 tmo5-like1* roots. Although the *tmo5 tmo5-like1* mutant showed reduced root and meristem length in control conditions compared to wild type, this did not result in altered root hair densities (**Fig. 2D** and **S14E-F**). This suggests that root and meristem length are not directly contributing to changes in root hair density. Fitting with the observed changes in root hair density, epidermal cell length was not different in wild type and *tmo5 tmo5-like1* under control conditions, was decreased in low phosphate conditions in wild type, and significantly less decreased in the *tmo5 tmo5-like1* double mutant (**Fig. 2E**). Similar results were obtained upon dGR induction (**Fig. 2E**). These results suggest that a reduction of epidermal cell length in the root hair zone drives the low phosphate response leading to an increase in root hair density.

TMO5/LHW dependent cytokinin controls root hair responses to low phosphate

To understand how TMO5/LHW in the xylem might be involved in the low phosphate response of root hairs in the epidermis, we analyzed expression of the transcriptional p*TMO5*::n3GFP reporter line (*28*). *TMO5* expression increased in response to low phosphate conditions (*29*) (**Fig. 3A, B**), consistent with the reported increase in auxin signaling under these limiting conditions (*22*) and the auxin-inducibility of *TMO5* (*2*). No ectopic expression of *TMO5* was observed in the trichoblast cells (**Fig. 3A)**. Furthermore, increasing TMO5 levels only in the xylem axis or in the vascular bundle (using p*TMO5*::TMO5:GR (*1*) or using newly generated p*SHR*::TMO5:GR and p*WOL*::XVE>>TMO5 lines), was sufficient to increase root hair density (**Fig. 3C-E** and **S17A-C**). This suggests that the effect of TMO5 on the low phosphate induced root hair density increase is cell non-autonomous.

The TMO5/LHW complex binds the *LOG4* promoter, thus promoting cytokinin biosynthesis. Cytokinin can then diffuse to neighboring cells where its perception induces cell proliferation (*1,*

6). To investigate if low phosphate conditions might lead to an increased induction of the cytokinin signaling pathway in epidermal cells, we analyzed the pTCSn::ntdTomato cytokinin-signaling reporter (*11, 30*). In low phosphate conditions, the TCSn reporter was induced in the epidermal cells of the root meristem (**Fig. 4A**). Additionally, A-type ARRs (including *ARR4, 5, 6, 8, 9, 12 and 15*), that our scRNA-seq dataset showed to be expressed in trichoblast cells, were upregulated upon TMO5/LHW induction (*11*) (**Fig. S13** and **S14A**). Additionally, expression of three trichoblast-restricted TMO5/LHW target genes was found to be induced by exogenous cytokinin treatment (**Fig. S18A**), fitting with published data (*31*). These results suggest an increased induction of the cytokinin signaling pathway in the epidermis under low phosphate conditions and fit with the published effect of cytokinin on cell length (*32*). To show that increased cytokinin levels and/or signaling might lead to an increase in root hair density due to a reduction in epidermal cell lengths, we next treated wild type roots with 0.1µM 6-benzylaminopurine, a synthetic cytokinin. Indeed, treatment with cytokinin in high phosphate conditions mimicked the root hair density promoting effect of low phosphate conditions (**Fig. 4B**) and a reduction in epidermal cell length (**Fig. S18B**). Additionally, cytokinin was sufficient to rescue the root hair density and epidermal cell length effects to low phosphate-like responses in the *tmo5 tmo5-like1* double mutant (**Fig. 4B** and **S18B**). To investigate the possible role of ethylene in this response (*33*), we next analyzed the responses of the *ein3 eil1* double mutant in downstream ethylene signaling on low phosphate medium and upon cytokinin treatment and found no difference compared to wild type plants (**Fig. S19A**), fitting with published reports that cytokinin effects on root hair length are not dependent on ethylene signaling (*34*) and the fact that ethylene response markers (*33*) were not uniformly altered upon TMO5/LHW induction (**Fig. S19B**). Given that the upstream *ein2* receptor single mutant does show some resistance to cytokinin but not low phosphate treatment (**Fig. S19A**), we cannot rule out involvement of complex cytokinin-ethylene hormonal cross-talk during this developmental process.

To provide additional genetic support for the hypothesis that cytokinin signaling in trichoblast cells drives the root hair response to low phosphate conditions in a TMO5-dependent manner, we first reduced cytokinin levels by analyzing the *log347* triple biosynthesis mutant (*8*) or by increasing levels of the CKX3 cytokinin conjugating enzyme (*35*) by analyzing a newly generated p*RPS5A*::CKX3 transgenic line. Both genetic tools to reduce cytokinin levels resulted in an inhibition of the low phosphate response (**Fig. 4C** and **S18C**). To strengthen that vascular-derived cytokinin is responsible for the root hair response to low phosphate conditions, we generated a vascular specific estradiol inducible *LOG4* transgenic line (p*WOL*::XVE>>LOG4). Upon induction of the cytokinin biosynthetic gene *LOG4* only in the vascular domain, an increase in root hair density was observed (**Fig. 4D**). Additionally, we complemented the *log 1234578* heptuple mutant (*9*),which has very low levels of active cytokinin, with *LOG4* expressed only in the TMO5 domain (*1*). In phosphate limiting conditions, p*TMO5*::LOG4 expression was sufficient to restore a wild type-like response (**Fig. S20**). Taken together, these experiments show that vascular-derived cytokinin is capable of triggering responses in the trichoblast cells. Thus, vascular-derived cytokinin can drive the root hair response to low phosphate conditions in a TMO5-dependent manner.

Previously, prolonged low phosphate conditions were shown to increase the number of cortex cell files and modify epidermal cell fates (*36*). To understand if these parameters might contribute to our observed increase in root hair density, we first analyzed the number of cells in radial sections of cortex and epidermal cell files as these determine the number of root hairs (*36*). Although prolonged growth in phosphate deprived conditions leads to an increase in the number

of cortex cells (*36*) (**Fig. S21**), this was not observed after 10 days, a time point used in all our experiments (**Table S2**); suggesting that the effects observed in our experiments are not due to additional cortex cells. We next examined the possible change in cell fate by examination of epidermal cell identity using markers for hair (p*COBL9*::GFP) (*37*) and non-hair (p*GL2*::GFP) (*38*) cell files. Epidermal cell identities were mixed upon cytokinin treatment, similar to the effect of low phosphate conditions (**Fig. 5A-C**) (*36*). This cytokinin-dependent effect most likely feeds into the known pathways determining epidermal cell identity, as cytokinin treatment was not able to induce hair formation in the *cpc try* double mutant (**Fig. S22**) (*39*). Moreover, significantly more root hairs were formed in non-hair positions upon dGR induction, exogenous cytokinin treatment and low phosphate conditions (**Fig. 5D**). This low phosphate effect was absent in the *tmo5 tmo5-like1* mutant and in plants with reduced cytokinin signaling levels (**Fig. 5D, E**). These results suggest that alterations in the epidermal cell identity contribute to the observed increase in root hair density upon low phosphate conditions.

Outlook

Here we showed that the vascular bHLH heterodimer TMO5/LHW controls root hair density by modifying epidermal cell length and cell fates. Phosphate deficit may trigger increased auxin signaling in xylem cells, inducing the TMO5/LHW pathway and downstream local cytokinin biosynthesis. Cytokinin may then diffuse outwards to direct length and fates of outer trichoblast cells. As such, this hormone signaling cascade spans multiple tissue layers in the meristem to regulate roots foraging for phosphate.

Acknowledgments: The authors would like to thank Veronique Storme for help with statistical analyses and Dolf Weijers for the use of unpublished materials. This work was supported by funding from the European Research Council (ERC Starting Grant TORPEDO; 714055), the Research Foundation - Flanders (FWO; Odysseus II G0D0515N); Ghent University (BOF20/GOA/012 and BOF18/PDO/151) and a Marie Curie Fellowship (IEF-2009-252503).

Author contributions: B.D.R., Y.S. and G.V.I. conceived the project; B.D.R., J.R.W. and B.Y. designed experiments; J.R.W., J.V.D., B.D.R. and G.V.I. generated samples for scRNA-seq; N.V.D. performed single cell RNA sequencing; N.V.D., K.V. and Y.S. analyzed scRNA-seq data and trajectory analysis; K.V. generated the on-line browser tool; W.S., B.W., E.M., H.E.A., J.N., B.Y. and J.R.W. generated reporter lines to validate the dataset; S.M. performed ploidy analysis; B.Y., C.V.d.V, M.M. and J.R.W. analyzed effects on root hair growth; B.D.R. and Y.S. supervised the project; B.D.R. wrote the paper with input from all authors.

Declaration of interests: The authors declare no conflict of interest related to this work

Data availability: The data can be accessed via a freely accessible on-line browser tool (http://bioit3.irc.ugent.be/plant-sc-atlas/) and raw data can be accessed at NCBI with GEO number: GSE141730. All other data are either in the main paper or the Supplement. Material requests should be directed to the corresponding authors.

Supplementary Materials:

Materials and Methods

Figures S1-S23

Tables S1-S3

References (1-66)

Figure Legends:

Figure 1: Identification of Arabidopsis root meristem cell types using scRNA-seq
A. Color-coded tSNE plot showing the classification of 5,145 high quality (UMI count > 17,290) cells into distinct cell identities corresponding to the schematic representation of the root meristem on the left. Grey dots represent predicted doublet cells. All inferred and validated developmental trajectories are projected onto the tSNE plot as black lines. Cells within dotted line are initials. QC: quiescent center, ppc: phloem procambium, se: sieve element, cc: companion cell, px: protoxylem, mx: metaxylem. **B.** Dot plot showing the expression of known tissue specific reporter genes in the scRNA-seq dataset, validating the annotation of tissue specific clusters. Size of the circles represents the percentage of cells with expression (pct.exp.), while the color indicates the scaled average expression (avg exp. scale). Dotted boxes represent major tissue types and cellular stages present in the root. **C.** Projection of predicted ploidy levels of each cell onto the tSNE plot.

Figure 2: TMO5 activity is required for root hair responses to low phosphate conditions
A. Number of TMO5/LHW target genes expressed in each of the tissue types of the Arabidopsis root meristem. Note the high number of trichoblast expressed genes. **B.** Predicted (left) and validated (right) expression of root hair specific target genes in the root hair. Arrowheads indicate nuclear expression. **C.** Root hair phenotype of dGR (induced or non-induced with dex) and wild type, *tmo5* single mutant and *tmo5 tmo5like1* double mutants grown on control conditions (high phosphate) or phosphate limiting conditions (low phosphate). **D-E.** Quantification of the root hair density (D) and epidermal cell length (E) of the lines depicted in C. Lower case letters on top of boxplots indicate significantly different groups as determined by one-way ANOVA with post-hoc Tukey HSD testing ($p<0.001$); the number of individuals is shown at the bottom of the plot and biological repeats are indicated using different symbols.

Figure 3: Vascular TMO5/LHW expression increases root hair density
A-B. Expression (A) and quantification (B) of the p*TMO5*::n3GFP reporter line in the root meristem under high (HP) and low (LP) phosphate conditions by confocal microscopy. **C-E.** Root hair phenotype and quantification of wild type, p*TMO5*::TMO5:GR, p*SHR*::TMO5:GR and p*WOL*::XVE>>TMO5:YFP roots grown on high phosphate conditions or induced by dexamethasone or estradiol (see Fig 2 for wild type control). Lower case letters on top of boxplots indicate significantly different groups as determined by one-way ANOVA with post-hoc Tukey HSD testing ($p<0.001$ in C and E, $p<0.01$ in D); the number of individuals is shown at the bottom of the plot and biological repeats are indicated using different symbols.

Figure 4: TMO5/LHW dependent cytokinin triggers root hair responses
A. Expression and quantification of pTCSn::ntdTomato in the root meristem under high (HP) and low (LP) phosphate conditions by confocal microscopy. Asterisks indicates epidermal cell layer. **B.** Root hair phenotype and quantification of wild type and *tmo5 tmo5like1* roots grown on high phosphate conditions or induced by cytokinin (BAP). **C.** Root hair phenotype and quantification of wild type and *log347* and p*RPS5A*::CKX3 roots grown on high or low phosphate conditions. **D.** Root hair phenotype and quantification of p*WOL*::XVE>>LOG4:YFP roots grown high phosphate conditions or induced by estradiol (see Fig 3 for wild type control). Lower case letters on top of boxplots indicate significantly different groups as determined by

299 one-way ANOVA with post-hoc Tukey HSD testing ($p<0.001$); the number of individuals is
300 shown at the bottom of the plot and biological repeats are indicated using different symbols.
301
302 **Figure 5: Cytokinin scrambles epidermal cell identities**
303 **A.** Expression of p*COBL9*::GFP and p*GL2*::GFP in roots grown in high phosphate (HP),
304 cytokinin (BAP), or low phosphate (LP). **B-C.** Quantification of number of cells per mm of root
305 in non-hair (NH) or hair (H) positions with GFP expression. **D-E.** Quantification of the number
306 of cells in non-hair position that form root hairs, along one mm of root from dGR, wild type,
307 *tmo5*, *tmo5 tmo5l1*, *log347* or p*RPS5A*::CKX3 grown under indicated conditions. Lower case
308 letters on top of the boxplots indicate significantly different groups as determined by one-way
309 ANOVA with post-hoc Tukey HSD testing ($p<0.001$); the number of individuals is shown at the
310 bottom of the plot and biological repeats are indicated using different symbols.

References

1. B. De Rybel *et al.*, Plant development. Integration of growth and patterning during vascular tissue formation in Arabidopsis. *Science* **345**, 1255215 (2014).
2. B. De Rybel *et al.*, A bHLH complex controls embryonic vascular tissue establishment and indeterminate growth in Arabidopsis. *Dev Cell* **24**, 426-437 (2013).
3. K. Ohashi-Ito, D. C. Bergmann, Regulation of the Arabidopsis root vascular initial population by LONESOME HIGHWAY. *Development* **134**, 2959-2968 (2007).
4. K. Ohashi-Ito, M. Matsukawa, H. Fukuda, An atypical bHLH transcription factor regulates early xylem development downstream of auxin. *Plant Cell Physiol* **54**, 398-405 (2013).
5. K. Ohashi-Ito, M. Oguchi, M. Kojima, H. Sakakibara, H. Fukuda, Auxin-associated initiation of vascular cell differentiation by LONESOME HIGHWAY. *Development* **140**, 765-769 (2013).
6. K. Ohashi-Ito *et al.*, A bHLH complex activates vascular cell division via cytokinin action in root apical meristem. *Curr Biol* **24**, 2053-2058 (2014).
7. F. Vera-Sirera *et al.*, A bHLH-Based Feedback Loop Restricts Vascular Cell Proliferation in Plants. *Dev Cell* **35**, 432-443 (2015).
8. T. Kuroha *et al.*, Functional analyses of LONELY GUY cytokinin-activating enzymes reveal the importance of the direct activation pathway in Arabidopsis. *The Plant Cell* **21**, 3152-3169 (2009).
9. H. Tokunaga *et al.*, Arabidopsis lonely guy (LOG) multiple mutants reveal a central role of the LOG-dependent pathway in cytokinin activation. *The Plant journal* **69**, 355-365 (2012).
10. S. Miyashima *et al.*, Mobile PEAR transcription factors integrate positional cues to prime cambial growth. *Nature* **565**, 490-494 (2019).
11. W. Smet *et al.*, DOF2.1 Controls Cytokinin-Dependent Vascular Cell Proliferation Downstream of TMO5/LHW. *Current biology : CB* **29**, 520-529 e526 (2019).
12. K. Jean-Baptiste *et al.*, Dynamics of Gene Expression in Single Root Cells of Arabidopsis. *Plant Cell* **31**, 993-1011 (2019).
13. T. Denyer *et al.*, Spatiotemporal Developmental Trajectories in the Arabidopsis Root Revealed Using High-Throughput Single-Cell RNA Sequencing. *Dev Cell* **48**, 840-852.e845 (2019).
14. T. Q. Zhang, Z. G. Xu, G. D. Shang, J. W. Wang, A Single-Cell RNA Sequencing Profiles the Developmental Landscape of Arabidopsis Root. *Mol Plant* **12**, 648-660 (2019).
15. K. H. Ryu, L. Huang, H. M. Kang, J. Schiefelbein, Single-Cell RNA Sequencing Resolves Molecular Relationships Among Individual Plant Cells. *Plant Physiol* **179**, 1444-1456 (2019).
16. C. N. Shulse *et al.*, High-Throughput Single-Cell Transcriptome Profiling of Plant Cell Types. *Cell Rep* **27**, 2241-2247.e2244 (2019).
17. S. Li, M. Yamada, X. Han, U. Ohler, P. N. Benfey, High-Resolution Expression Map of the Arabidopsis Root Reveals Alternative Splicing and lincRNA Regulation. *Dev Cell* **39**, 508-522 (2016).
18. R. Ruonala, D. Ko, Y. Helariutta, Genetic Networks in Plant Vascular Development. *Annu Rev Genet* **51**, 335-359 (2017).
19. A. Rodriguez-Villalon *et al.*, Molecular genetic framework for protophloem formation. *Proc Natl Acad Sci U S A* **111**, 11551-11556 (2014).

20. A. P. Mähönen *et al.*, A novel two-component hybrid molecule regulates vascular morphogenesis of the Arabidopsis root. *Genes & development* **14**, 2938-2943 (2000).
21. R. Bhosale *et al.*, A Spatiotemporal DNA Endoploidy Map of the Arabidopsis Root Reveals Roles for the Endocycle in Root Development and Stress Adaptation. *Plant Cell* **30**, 2330-2351 (2018).
22. R. Bhosale *et al.*, A mechanistic framework for auxin dependent Arabidopsis root hair elongation to low external phosphate. *Nat Commun* **9**, 1409 (2018).
23. J. E. Salazar-Henao, I. C. Vélez-Bermúdez, W. Schmidt, The regulation and plasticity of root hair patterning and morphogenesis. *Development* **143**, 1848-1858 (2016).
24. M. Grebe *et al.*, Cell polarity signaling in Arabidopsis involves a BFA-sensitive auxin influx pathway. *Curr Biol* **12**, 329-334 (2002).
25. H. Rouached, A. B. Arpat, Y. Poirier, Regulation of phosphate starvation responses in plants: signaling players and cross-talks. *Mol Plant* **3**, 288-299 (2010).
26. Z. H. Chen, G. A. Nimmo, G. I. Jenkins, H. G. Nimmo, BHLH32 modulates several biochemical and morphological processes that respond to Pi starvation in Arabidopsis. *Biochem J* **405**, 191-198 (2007).
27. Z. Ma, D. G. Bielenberg, K. M. Brown, J. P. Lynch, Regulation of root hair density by phosphorus availability in *Arabidopsis thaliana*. *Plant Cell and Environment* **24**, 459-467 (2001).
28. A. Schlereth *et al.*, MONOPTEROS controls embryonic root initiation by regulating a mobile transcription factor. *Nature* **464**, 913-916 (2010).
29. P. Wu *et al.*, Phosphate starvation triggers distinct alterations of genome expression in Arabidopsis roots and leaves. *Plant Physiol* **132**, 1260-1271 (2003).
30. E. Zurcher *et al.*, A robust and sensitive synthetic sensor to monitor the transcriptional output of the cytokinin signaling network in planta. *Plant Physiology* **161**, 1066-1075 (2013).
31. K. C. Potter, J. Wang, G. E. Schaller, J. J. Kieber, Cytokinin modulates context-dependent chromatin accessibility through the type-B response regulators. *Nat Plants* **4**, 1102-1111 (2018).
32. I. H. Street *et al.*, Cytokinin acts through the auxin influx carrier AUX1 to regulate cell elongation in the root. *Development* **143**, 3982-3993 (2016).
33. L. Song *et al.*, The Molecular Mechanism of Ethylene-Mediated Root Hair Development Induced by Phosphate Starvation. *PLoS Genet* **12**, e1006194 (2016).
34. S. Zhang *et al.*, Multiple phytohormones promote root hair elongation by regulating a similar set of genes in the root epidermis in Arabidopsis. *J Exp Bot* **67**, 6363-6372 (2016).
35. T. Schmülling, T. Werner, M. Riefler, E. Krupková, I. Bartrina y Manns, Structure and function of cytokinin oxidase/dehydrogenase genes of maize, rice, Arabidopsis and other species. *J Plant Res* **116**, 241-252 (2003).
36. G. Janes *et al.*, Cellular Patterning of Arabidopsis Roots Under Low Phosphate Conditions. *Front Plant Sci* **9**, 735 (2018).
37. S. M. Brady, S. Song, K. S. Dhugga, J. A. Rafalski, P. N. Benfey, Combining expression and comparative evolutionary analysis. The COBRA gene family. *Plant Physiol* **143**, 172-187 (2007).
38. Y. Lin, J. Schiefelbein, Embryonic control of epidermal cell patterning in the root and hypocotyl of Arabidopsis. *Development* **128**, 3697-3705 (2001).

39. M. Simon, M. M. Lee, Y. Lin, L. Gish, J. Schiefelbein, Distinct and overlapping roles of single-repeat MYB genes in root epidermal patterning. *Dev Biol* **311**, 566-578 (2007).

Supplementary References

40. M. Bonke, S. Thitamadee, A. P. Mahonen, M. T. Hauser, Y. Helariutta, APL regulates vascular tissue identity in Arabidopsis. *Nature* **426**, 181-186 (2003).
41. J. M. Alonso, T. Hirayama, G. Roman, S. Nourizadeh, J. R. Ecker, EIN2, a bifunctional transducer of ethylene and stress responses in Arabidopsis. *Science* **284**, 2148-2152 (1999).
42. T. Potuschak *et al.*, EIN3-dependent regulation of plant ethylene hormone signaling by two arabidopsis F box proteins: EBF1 and EBF2. *Cell* **115**, 679-689 (2003).
43. M. K. Zhiponova *et al.*, Helix-loop-helix/basic helix-loop-helix transcription factor network represses cell elongation in Arabidopsis through an apparent incoherent feed-forward loop. *Proc Natl Acad Sci U S A* **111**, 2824-2829 (2014).
44. J. Goossens, G. Swinnen, R. Vanden Bossche, L. Pauwels, A. Goossens, Change of a conserved amino acid in the MYC2 and MYC3 transcription factors leads to release of JAZ repression and increased activity. *New Phytol* **206**, 1229-1237 (2015).
45. A. Coego *et al.*, The TRANSPLANTA collection of Arabidopsis lines: a resource for functional analysis of transcription factors based on their conditional overexpression. *Plant J* **77**, 944-953 (2014).
46. A. S. Iyer-Pascuzzi, P. N. Benfey, Fluorescence-activated cell sorting in plant developmental biology. *Methods Mol Biol* **655**, 313-319 (2010).
47. A. T. Lun, K. Bach, J. C. Marioni, Pooling across cells to normalize single-cell RNA sequencing data with many zero counts. *Genome Biol* **17**, 75 (2016).
48. A. T. Lun, D. J. McCarthy, J. C. Marioni, A step-by-step workflow for low-level analysis of single-cell RNA-seq data with Bioconductor. *F1000Res* **5**, 2122 (2016).
49. C. S. McGinnis, L. M. Murrow, Z. J. Gartner, DoubletFinder: Doublet Detection in Single-Cell RNA Sequencing Data Using Artificial Nearest Neighbors. *Cell Syst* **8**, 329-337.e324 (2019).
50. K. Birnbaum *et al.*, A gene expression map of the Arabidopsis root. *Science (New York, N.Y* **302**, 1956-1960 (2003).
51. W. Saelens, R. Cannoodt, H. Todorov, Y. Saeys, A comparison of single-cell trajectory inference methods. *Nat Biotechnol* **37**, 547-554 (2019).
52. K. Street *et al.*, Slingshot: cell lineage and pseudotime inference for single-cell transcriptomics. *BMC Genomics* **19**, 477 (2018).
53. L. Muñiz *et al.*, ACAULIS5 controls Arabidopsis xylem specification through the prevention of premature cell death. *Development* **135**, 2573-2582 (2008).
54. A. Carlsbecker *et al.*, Cell signalling by microRNA165/6 directs gene dose-dependent root cell fate. *Nature* **465**, 316-321 (2010).
55. M. Kubo *et al.*, Transcription switches for protoxylem and metaxylem vessel formation. *Genes Dev* **19**, 1855-1860 (2005).
56. M. Taylor-Teeples *et al.*, An Arabidopsis gene regulatory network for secondary cell wall synthesis. *Nature* **517**, 571-575 (2015).
57. S. Otero, Y. Helariutta, Companion cells: a diamond in the rough. *J Exp Bot* **68**, 71-78 (2017).

58. V. López-Salmerón, H. Cho, N. Tonn, T. Greb, The Phloem as a Mediator of Plant Growth Plasticity. *Curr Biol* **29**, R173-R181 (2019).
59. J. R. Wendrich, C. Y. Liao, W. A. van den Berg, B. De Rybel, D. Weijers, Ligation-independent cloning for plant research. *Methods Mol Biol* **1284**, 421-431 (2015).
60. R. Siligato *et al.*, MultiSite Gateway-Compatible Cell Type-Specific Gene-Inducible System for Plants. *Plant Physiol* **170**, 627-641 (2016).
61. S. J. Clough, A. F. Bent, Floral dip: a simplified method for Agrobacterium-mediated transformation of Arabidopsis thaliana. *Plant Journal* **16**, 735-743 (1998).
62. R. Ursache, T. G. Andersen, P. Marhavý, N. Geldner, A protocol for combining fluorescent proteins with histological stains for diverse cell wall components. *Plant J* **93**, 399-412 (2018).
63. E. Truernit *et al.*, High-resolution whole-mount imaging of three-dimensional tissue organization and gene expression enables the study of Phloem development and structure in Arabidopsis. *The Plant Cell* **20**, 1494-1503 (2008).
64. P. Barbier de Reuille *et al.*, MorphoGraphX: A platform for quantifying morphogenesis in 4D. *Elife* **4**, 05864 (2015).
65. B. De Rybel *et al.*, A novel Aux/IAA28 signaling cascade activates GATA23-dependent specification of lateral root founder cell identity. *Current biology* **20**, 1697-1706 (2010).
66. H. Wickham, *ggplot2, Elegant Graphics for Data Analysis*. Use R! (Springer-Verlag New York, 2009), vol. 1, pp. VIII, 213.

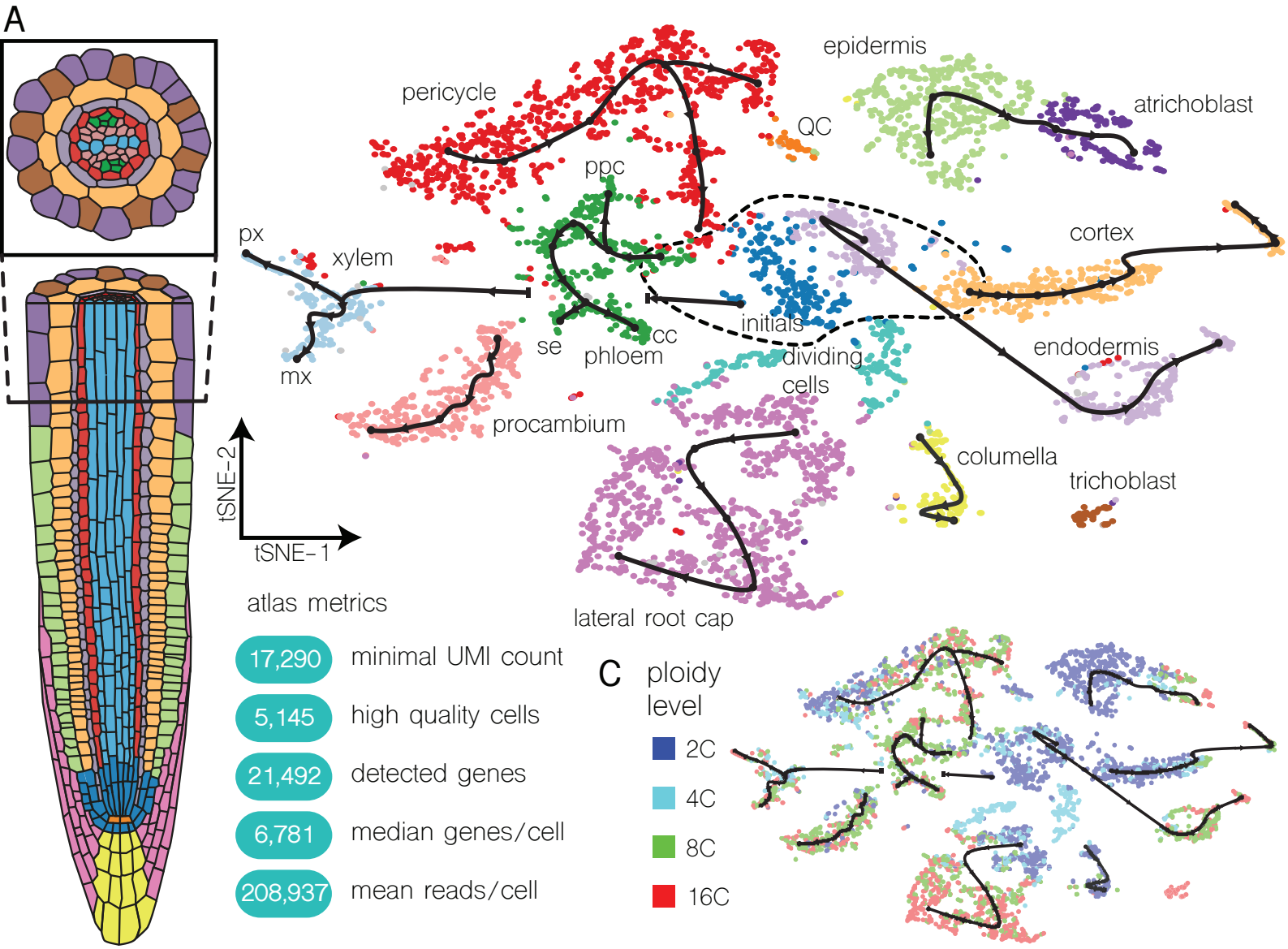
A
pericycle
epidermis
atrichoblast
QC
ppc
px
xylem
cortex
initials
cc
se
phloem
endodermis
mx
dividing
cells
procambium
columella
trichoblast
tSNE-2
tSNE-1
lateral root cap
atlas metrics
17,290
minimal UMI count
5,145
high quality cells
21,492
detected genes
6,781
median genes/cell
208,937
mean reads/cell
C
ploidy
level
2C
4C
8C
16C

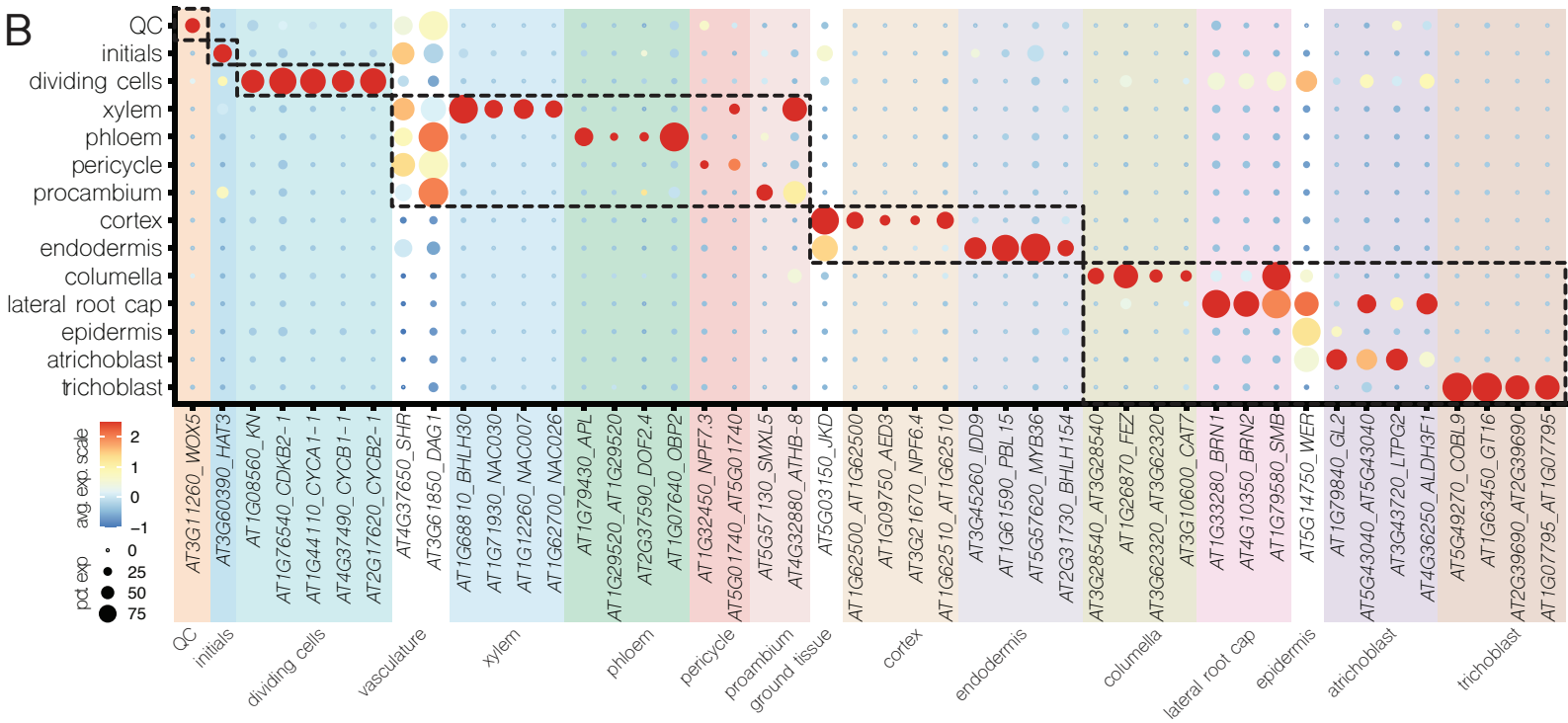
B
QC
initials
dividing cells
xylem
phloem
pericycle
procambium
cortex
endodermis
columella
lateral root cap
epidermis
atrichoblast
trichoblast
avg. exp. scale
2
1
0
−1
pct. exp.
0
25
50
75
AT3G11260_WOX5
AT3G60390_HAT3
AT1G08560_KN
AT1G76540_CDKB2-1
AT1G44110_CYCA1-1
AT4G37490_CYCB1-1
AT2G17620_CYCB2-1
AT4G37650_SHR
AT3G61850_DAG1
AT1G68810_BHLH30
AT1G71930_NAC030
AT1G12260_NAC007
AT1G62700_NAC026
AT1G79430_APL
AT1G29520_AT1G29520
AT2G37590_DOF2.4
AT1G07640_OBP2
AT1G32450_NPF7.3
AT5G01740_AT5G01740
AT5G57130_SMXL5
AT4G32880_ATHB-8
AT5G03150_JKD
AT1G62500_AT1G62500
AT1G09750_AED3
AT3G21670_NPF6.4
AT1G62510_AT1G62510
AT3G45260_IDD9
AT1G61590_PBL15
AT5G57620_MYB36
AT2G31730_BHLH154
AT3G28540_AT3G28540
AT1G26870_FEZ
AT3G62320_AT3G62320
AT3G10600_CAT7
AT1G33280_BRN1
AT4G10350_BRN2
AT1G79580_SMB
AT5G14750_WER
AT1G79840_GL2
AT5G43040_AT5G43040
AT3G43720_LTPG2
AT4G36250_ALDH3F1
AT5G49270_COBL9
AT1G63450_GT16
AT2G39690_AT2G39690
AT1G07795_AT1G07795
QC
initials
dividing cells
vasculature
xylem
phloem
pericycle
procambium
ground tissue
cortex
endodermis
columella
lateral root cap
epidermis
atrichoblast
trichoblast

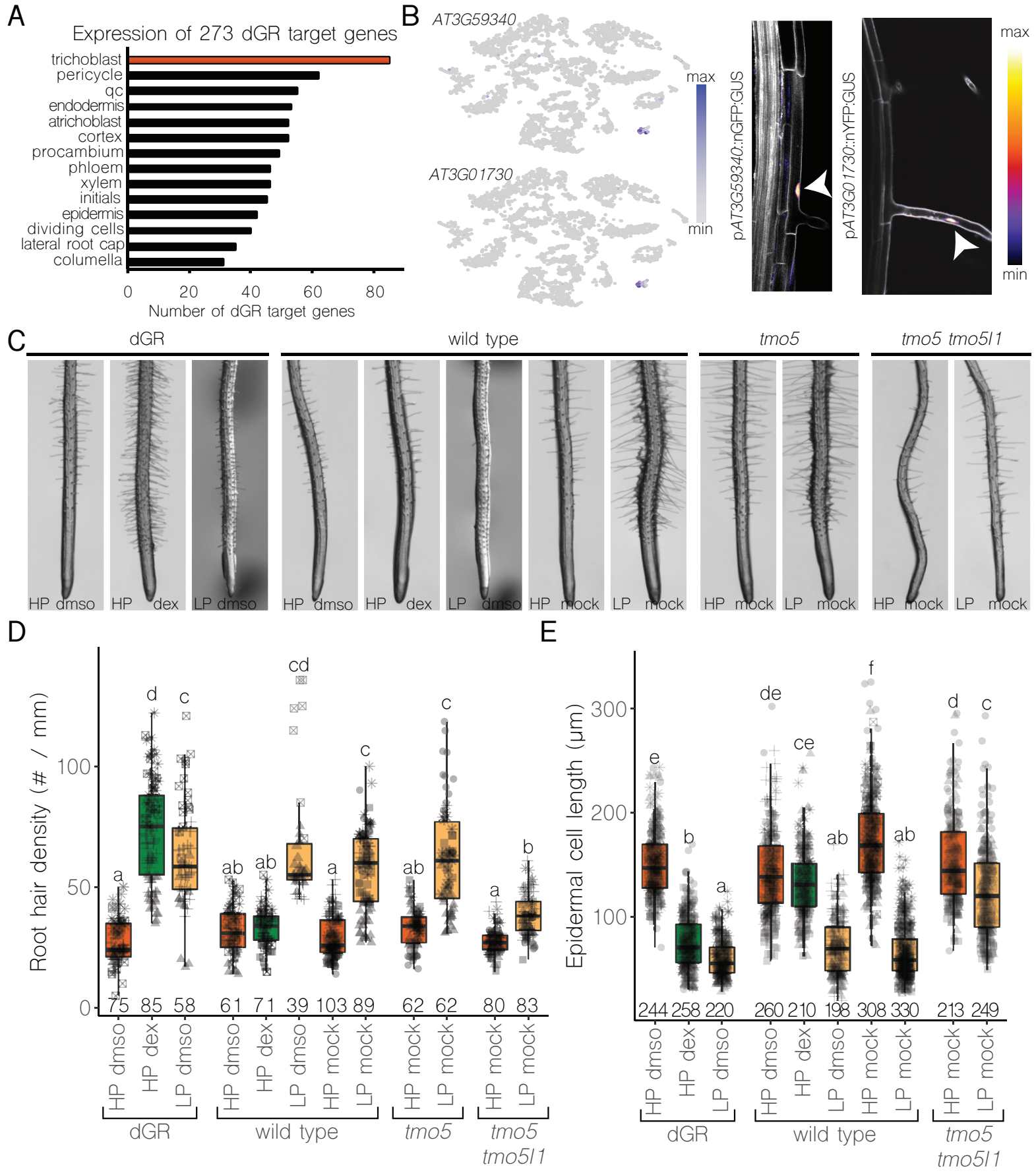
A
Expression of 273 dGR target genes
trichoblast
pericycle
qc
endodermis
atrichoblast
cortex
procambium
phloem
xylem
initials
epidermis
dividing cells
lateral root cap
columella
0
20
40
60
80
Number of dGR target genes
B
AT3G59340
AT3G01730
max
min
pAT3G59340::nGFP:GUS
pAT3G01730::nYFP:GUS
max
min
C
dGR
wild type
tmo5
tmo5 tmo5l1
HP dmso
HP dex
LP dmso
HP dmso
HP dex
LP dmso
HP mock
LP mock
HP mock
LP mock
HP mock
LP mock
D
Root hair density (# / mm)
0
50
100
a
d
c
ab
ab
cd
a
c
ab
c
a
b
75
85
58
61
71
39
103
89
62
62
80
83
HP dmso
HP dex
LP dmso
HP dmso
HP dex
LP dmso
HP mock
LP mock
HP mock
LP mock
HP mock
LP mock
dGR
wild type
tmo5
tmo5
tmo5l1
E
Epidermal cell length (µm)
100
200
300
e
b
a
de
ce
ab
f
ab
d
c
244
258
220
260
210
198
308
330
213
249
HP dmso
HP dex
LP dmso
HP dmso
HP dex
LP dmso
HP mock
LP mock
HP mock
LP mock
dGR
wild type
tmo5
tmo5
tmo5l1

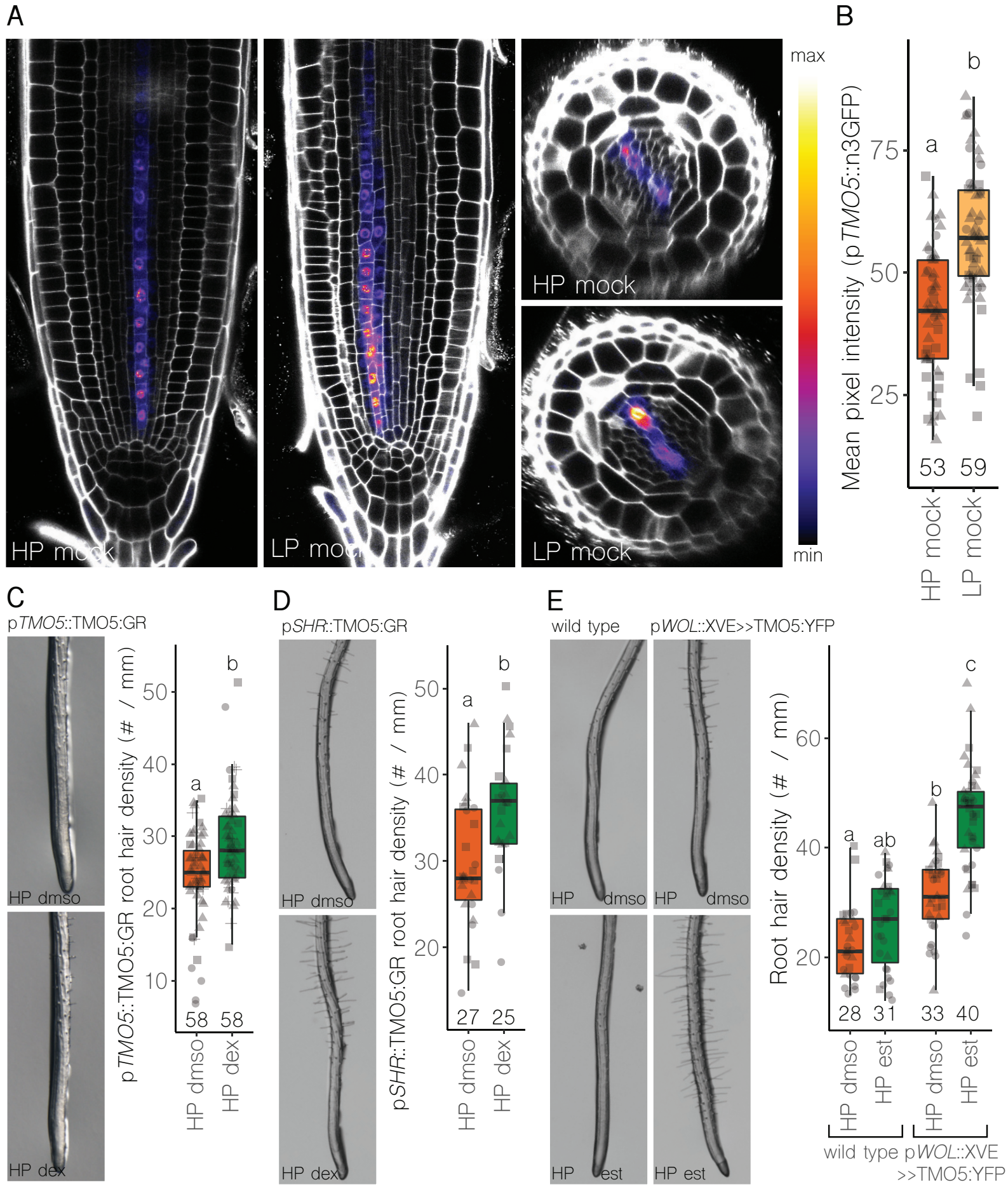
A
HP mock
LP mock
HP mock
LP mock
max
min
B
Mean pixel intensity (pTMO5::n3GFP)
75
50
25
a
b
53
59
HP mock
LP mock
C
pTMO5::TMO5:GR
HP dmso
HP dex
pTMO5::TMO5:GR root hair density (# / mm)
50
40
30
20
10
a
b
58
58
HP dmso
HP dex
D
pSHR::TMO5:GR
HP dmso
HP dex
pSHR::TMO5:GR root hair density (# / mm)
50
40
30
20
a
b
27
25
HP dmso
HP dex
E
wild type
pWOL::XVE>>TMO5:YFP
HP dmso
HP dmso
HP est
HP est
Root hair density (# / mm)
60
40
20
a
ab
b
c
28
31
33
40
HP dmso
HP est
HP dmso
HP est
wild type
pWOL::XVE >>TMO5:YFP

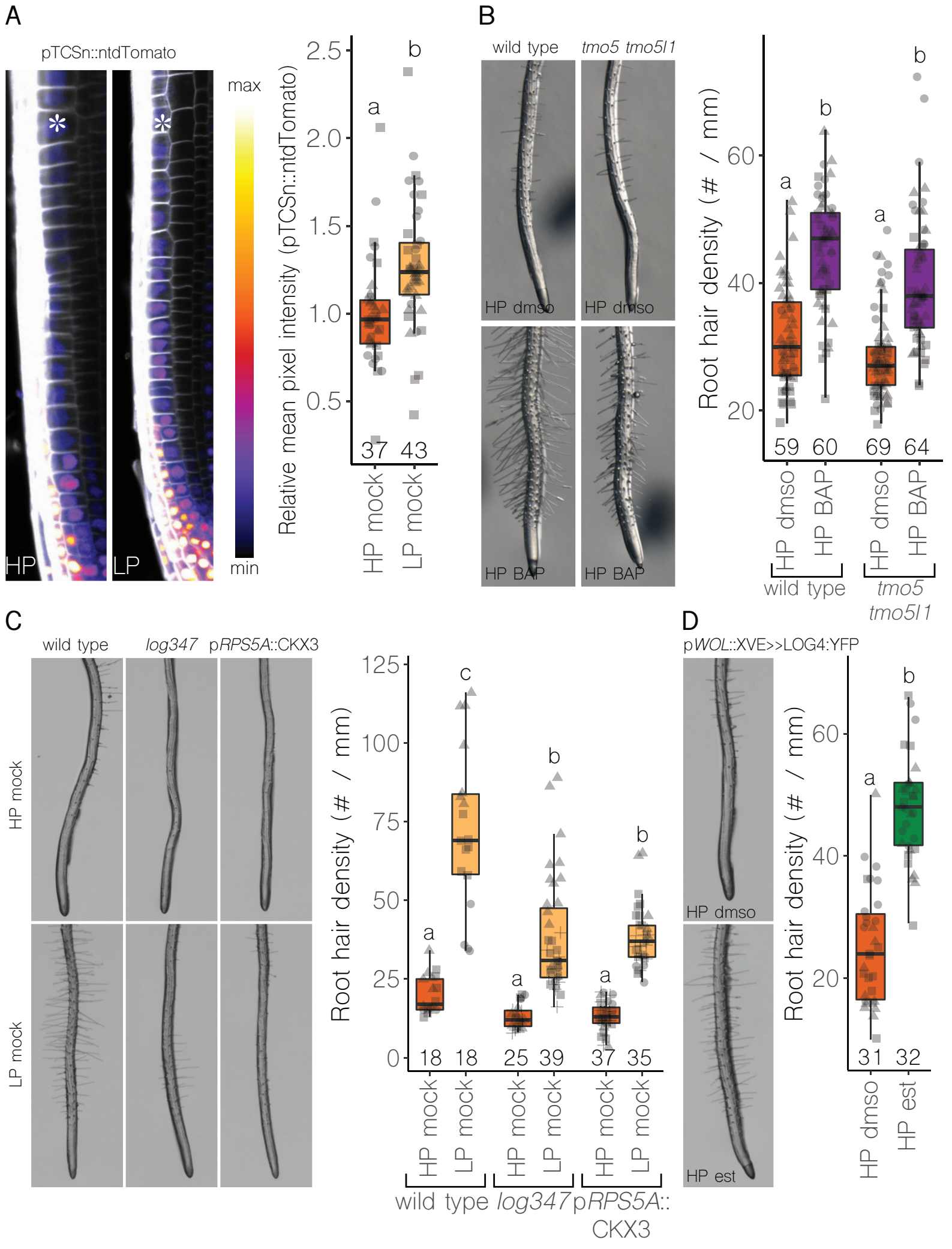
A
pTCSn::ntdTomato
max
min
HP
LP
Relative mean pixel intensity (pTCSn::ntdTomato)
2.5
2.0
1.5
1.0
0.5
a
b
37
43
HP mock
LP mock
B
wild type
tmo5 tmo5l1
HP dmso
HP dmso
HP BAP
HP BAP
Root hair density (# / mm)
60
40
20
a
b
a
b
59
60
69
64
HP dmso
HP BAP
HP dmso
HP BAP
wild type
tmo5 tmo5l1
C
wild type
log347
pRPS5A::CKX3
HP mock
LP mock
Root hair density (# / mm)
125
100
75
50
25
0
a
c
a
b
a
b
18
18
25
39
37
35
HP mock
LP mock
HP mock
LP mock
HP mock
LP mock
wild type
log347
pRPS5A::
CKX3
D
pWOL::XVE>>LOG4:YFP
HP dmso
HP est
Root hair density (# / mm)
60
40
20
a
b
31
32
HP dmso
HP est

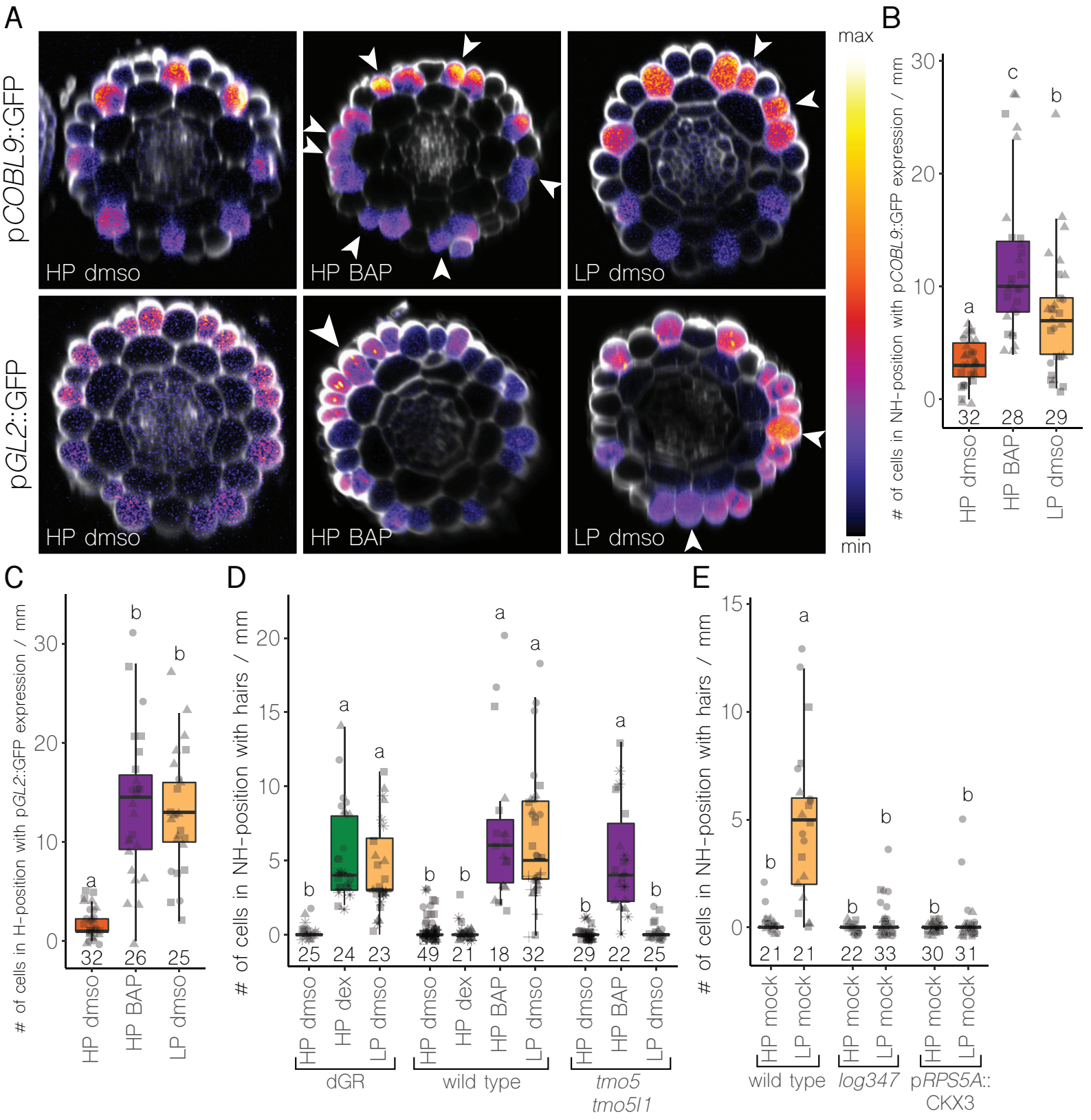
A
pCOBL9::GFP
pGL2::GFP
HP dmso
HP BAP
LP dmso
HP dmso
HP BAP
LP dmso
max
min
B
# of cells in NH-position with pCOBL9::GFP expression / mm
30
20
10
0
a
c
b
32
28
29
HP dmso
HP BAP
LP dmso
C
# of cells in H-position with pGL2::GFP expression / mm
30
20
10
0
a
b
b
32
26
25
HP dmso
HP BAP
LP dmso
D
# of cells in NH-position with hairs / mm
20
15
10
5
0
b
a
a
b
b
b
a
a
b
b
a
25
24
23
49
21
18
32
29
22
25
HP dmso
HP dex
LP dmso
HP dmso
HP dex
HP BAP
LP dmso
HP dmso
HP BAP
LP dmso
dGR
wild type
tmo5
tmo5l1
E
# of cells in NH-position with hairs / mm
15
10
5
0
b
a
b
b
b
b
21
21
22
33
30
31
HP mock
LP mock
HP mock
LP mock
HP mock
LP mock
wild type
log347
pRPS5A::
CKX3

Science
AAAS

Supplementary Materials for

Vascular transcription factors guide plant epidermal responses to limiting phosphate conditions

Jos R. Wendrich[1,2,†], BaoJun Yang[1,2,†], Niels Vandamme[3,4,†], Kevin Verstaen[3,4,†], Wouter Smet[1,2], Celien Van de Velde[1,2], Max Minne[1,2], Brecht Wybouw[1,2], Eliana Mor[1,2], Helena E. Arents[1,2], Jonah Nolf[1,2], Julie Van Duyse[5,6], Gert Van Isterdael[5,6], Steven Maere[1,2], Yvan Saeys[3,4,*] and Bert De Rybel[1,2,*]

Correspondence to: Bert De Rybel (beryb@psb.vib-ugent.be) and Yvan Saeys (yvan.saeys@irc.vib-ugent.be)

This PDF file includes:

Other Supplementary Materials for this manuscript include the following:

Materials and Methods

Plant material and growth conditions

All seeds were surface sterilized, sown on solid ½ MS plates without sucrose, and stratified at 4°C two days before they were grown at 22°C in continuous light conditions. Ten-day old seedlings were transferred to soil and grown in green house conditions. For phosphate limiting experiments, plants were grown for 10 days on plates containing ½ modified MS salts (M407 – Phyto Technology Laboratories), 0.55 mM myo-inositol, 20.6 mM NH_4NO_3, 18.8 mM KNO_3, 0.8% washed agar and 1.25 mM or 100 µM KH_2PO_4 (for "high phosphate; HP" or "low phosphate; LP", respectively). Dexamethasone (dex) treatment was performed by either germinating seeds on 10 µM dex-supplemented medium or by transferring plants from ½ MS to 10 µM dex supplemented medium and continuing growth for the indicated time. 6-Benzylaminopurine (BAP) and beta-estradiol (est) treatments were performed by germination on plates supplemented with 0.1 µM BAP or 10 µM est, respectively. BAP, dex and est were dissolved in dimethyl sulfoxide as solvent (DMSO, 10 mM stock solutions each). Addition of DMSO to the medium was found to have an effect on root hair length, largely canceling out the effect of limiting phosphate conditions on hair length. This effect was limited to hair length, as a large phosphate-dependent effect could still be observed at the level of root hair density (**Fig. S23**). Media containing no additives is referred to as "mock". The *Arabidopsis thaliana* (L.) Heynh. Col-0 ecotype served as wild-type control in all experiments, unless otherwise stated. Plant lines used in this study: p*RPS5A*::TMO5:GR-p*RPS5A*::LHW:GR or dGR (*11*), p*TMO5*::n3GFP (*28*), pTCSn::ntdTomato (*11*), *tmo5* (*2*), *tmo5 tmo5l1* (*2*), *log3 log4 log7* (*8*), *log 1234578 heptuple* mutant (*9*), p*TMO5*::LOG4 in *log 1234578 heptuple* mutant (*1*), p*COBL9*::GFP (*37*), p*GL2*::GFP (*38*), p*WOL*::erGFP (*40*), *ein2* (*41*), *ein3 eil1* (*42*), p*GL2*::GUS in Ws ecotype (*39*), p*GL2*::GUS in *cpc try* double mutant (*39*), p*35S*::IBH1 (*43*), p*35S*::IBL1 (*43*), p*35S*::MYC2 (*44*), TRANSPLANTA lines: TPT_1.01260.2C, TPT_4.09180.1C, TPT_1.01260.2I, TPT_1.05805.1C, TPT_1.05805.1E, TPT_1.05805.1H, TPT_1.62975.1A, TPT_1.62975.1B, TPT_1.62975.1D, TPT_1.62975.1F, TPT_1.62975.1H, TPT_1.62975.1I, TPT_1.68920.2A, TPT_1.68920.2F, TPT_2.18300.1B, TPT_2.18300.1C, TPT_2.18300.1I, TPT_2.22750.2G, TPT_4.09180.1B, TPT_1.01260.2G (*45*).

Protoplasting conditions and FACS

Protoplasting was performed as described previously (*46*) with minor modifications. Briefly, root tips of 6-d-old seedlings were cut and incubated in protoplasting Solution B [1.5% (wt/vol) cellulysin and 0.1% (wt/vol) pectolyase in Solution A (600 mM mannitol, 2 mM $MgCl_2$, 0.1% [wt/vol] BSA, 2 mM $CaCl_2$, 2 mM MES, 10mM KCl, pH 5.5)] for approximately 1 h at room temperature. Conditions were optimized to ensure the inner vascular cell types were dissociated well (even if this was to some extent at the expense of the outer cell files) by microscopic analysis of the protoplasting at regular intervals. Cells were filtered through a 70 µm cell strainer and spun down at 200 × g for 6 min; resuspended in Solution A, filtered through a 40 µm cell strainer and stained for live/dead using 4′,6-diamidino-2-phenylindole (DAPI) at 14 µM final concentration. Cells were sorted on a BD Aria II, and protoplasts not containing the DAPI signal were selected for further analysis.

10X Genomics sample preparation, library construction and sequencing

Sorted cells were centrifuged at 4°C at 400g and resuspended in PBS+0,04%BSA to yield an estimated concentration of 1000 cells/µl, before being subdivided to generate three replicates that have gone through the rest of the pipeline as independent samples. Cellular suspensions were loaded on a GemCode Single Cell 3' Gel Bead and Library Kit (V2 chemistry, 10X

Genomics) according to the manufacturer's instructions. Sequencing libraries were loaded on an Illumina HiSeq4000 and sequenced following recommendations of 10X Genomics at the VIB Nucleomics Core (VIB, Leuven).

Raw data processing and generation of gene expression matrix

Demultiplexing of the raw sequencing data was done by the 10x CellRanger (version 2.0.2) software 'cellranger mkfastq' which wraps Illumina's bcl2fastq. The fastq files obtained after demultiplexing were used as the input for 'cellranger count' which align the reads to the *Arabidopsis thaliana* reference genome (Ensemble TAIR10.40) using STAR and collapses them to unique molecular identifier (UMI) counts. The result is a large digital expression matrix with cell barcodes as rows and gene identities as columns. The aggregation of the replicate samples was done using 'cellranger aggr'. Initial filtering in CellRanger (gene count > 200), recovered 15,918 cells. To ensure we only use high-quality cells for further analysis, we used the filtered data provided by cellranger. This corresponds to a minimum UMI count of 17,290 in the aggregated data, recovering a final 5,145 cells.

Data Analysis (Clustering, Identity Assignment, DEG, and Quality Control)

All analyses were performed in R (version 3.5.2). Pre-processing of the data was done by the scran (version 1.10.1) and scater (version 1.10.1) packages according to the workflow proposed by the Marioni lab (*47*). Outlier cells were identified based on 2 metrics (library size and number of expressed genes) and were tagged as outliers when they were 3 median absolute deviation (MADs) away from the median value of these metrics across all cells. Low-abundance genes were removed using the 'calcAverage' function and the proposed workflow by Satija and colleagues (*48*). The raw counts were normalized and log2 transformed by first calculating "size factors" that represent the extent to which counts should be scaled in each library. Detecting highly variable genes, finding clusters and creating tSNE plots was done using the Seurat pipeline (version 2.3.4). Differential expression analysis for marker gene identification per subpopulation was based on the non-parametric Wilcoxon rank sum test implemented within the Seurat pipeline. Clusters with the same cell annotation based on gene expression analysis were combined to generate a more comprehensible dataset. The relative contribution of each replicate sample to the entire dataset and each individual cluster ranged between 28% and 38%, indicating reproducibility and limited batch effects (**Fig. S1C**). Potential doublets were identified using the DoubletFinder algorithm (version 2.0.0) (*49*). The number of high confidence doublets (indicated in grey on the tSNE plot in **Fig 1A**) was below 1% (50 out of 5,145 cells). To assess whether a capturing bias of meristem cells was introduced during protoplast isolation, Arabidopsis root meristems were imaged using 3D confocal microscopy (see Plant imaging section below). After segmentation, cells were quantified according to their individual identities and the *in vivo* proportions were compared to the proportions within the scRNA-seq dataset. Out of the total number of cells, we observed a 15% overrepresentation of the inner vascular cell types and a 13% underrepresentation of more outer cell layers (**Fig. S1D**). This was expected, as we optimized the protocol to distinguish inner vascular cells from other cells. No other selective capturing was apparent. The effect of protoplasting on gene expression (*50*) was limited to maximum 8% of the top 100 DEGs and only observed in the most outer tissue types of the root (**Fig. S1E**)

Data comparison

Comparison of different available *Arabidopsis* root scRNA-seq datasets (*12-15*) was done, revealing similarities and differences between these datasets, as shown below.

dataset	technology used	number of cells	average reads per cell	median genes per cell
Denyer et al., 2019 (*13*)	10X v2	4.727	87.000	4.276
Jean-Baptiste et al., 2019 (*12*)	10X	3.121	-	2.445
Zhang et al., 2019 (*14*)	10X v2	7.695	39.667	1.875
Ryu et al., 2019 (*15*)	10X v2	7.522	75.000	5.000
This study	10X v2	5.145	208.937	6.781

Pseudotime trajectory analysis

Pseudotime trajectory analysis was performed with different methods compiled in the Dyno R package (version 0.1.1) (*51*). The optimal method for each cell identity was selected based on prior biological knowledge and the guidelines in the Dyno package. The consensus trajectory was fixed after iterative and reproducible inference calculation. The GNG algorithm was used to infer trajectories for the following cell identities: phloem (seed set at 4), xylem (seed set at 2), cortex (seed set at 1), LRC + columella (seed set at 1), pericycle (seed set at 13); Slingshot was used for endodermis and cambium (*52*).

For trajectory inference on the xylem subpopulations, cells were ordered along a bifurcating trajectory from xylem initials towards protoxylem and metaxylem (**Fig. 3A**). The identification and validation of the subpopulations and branching points is based on gene expression of known regulators of xylem development such as *ACL5* and *ATHB15* for early metaxylem (*53, 54*); *TMO5* for early proto- and metaxylem (*2*); *VND2* for intermediate xylem (*55*); *VND7* and *CESA4* for late protoxylem (*55, 56*) (**Fig. S3A**). Although our method depends on generating protoplasts and is not efficient at retrieving differentiating cells, we acquired many genes involved in secondary cell wall formation in the protoxylem sub-cluster, but less so in the metaxylem sub-cluster. All newly generated reporter lines confirmed the predicted pseudotime and tissue specific expression patterns for the xylem trajectory (**Fig. S3B**).

For the phloem cell lineage, the GNG trajectory algorithm ordered the cells across five cellular states of phloem development with more elaborate branching (**Fig. S4A**). Known reporter genes (including *APL* for non-procambium (*57*), *JUL1* for procambium (*58*); the PEAR gene *DOF5.6* for sieve elements (*10*) and *SUC2* for companion cells (*57*)) confirmed predicted sub-cluster identities within the phloem developmental trajectories (**Fig. S4A**). Also for this more complex trajectory, all newly generated reporter lines confirmed the predicted spatiotemporal expression patterns (**Fig. S4B**).

A similar analysis and validation was performed on the predicted developmental trajectories and sub-cluster identities for the procambium, pericycle, endodermis, cortex, epidermis, lateral root cap and columella clusters (**Fig. S5-11**)

On-line tool for visualization of data

To allow optimal accessibility of this scRNA-seq dataset by the scientific community, cell type specific expression patterns of individual genes, expression levels along developmental trajectories and bulk downloads can be accessed via a freely accessible on-line browser tool (http://bioit3.irc.ugent.be/plant-sc-atlas/), which includes a warning flag for protoplast-induced genes.

Cell ploidy predictions

For predicting the ploidy of individual cells, we correlated the scRNA-seq dataset with a dataset of ploidy-specific gene expression levels in Arabidopsis root cortex tissue (*21*). The expression values of 332 previously established ploidy marker genes (Supplemental Table 5

in (*21*)) were standardized in both datasets separately (zero mean, unit variance), and Pearson correlation coefficients (PCC) were calculated between the resulting marker gene expression profile in each cell and the marker gene expression profiles of 2C, 4C, 8C and 16C cells in the cortex dataset. The predicted ploidy level of a given cell was then taken to be the ploidy level for which the PCC between the cortex and cell data was maximal.

Gene selection, cloning and plant transformation

Genes from the top 20 differentially expressed genes per cell type were selected based on predicted unique expression after manual curation of the feature plots. Transcriptional reporter lines were obtained by amplifying the upstream region of the transcriptional start and cloning this into the pDONRP41R entry vector. The final expression clones were generated by cloning the promoter regions into the pBGWFS7 destination vector using Gateway cloning. Only lines with stable expression patterns in at least 10 independent transformants were kept, resulting in a set of 41 novel transcriptional reporter lines. p*TMO5*::TMO5:GR line was generated by first generating a LIC-compatible vector containing *TMO5* promoter, after which TMO5:GR was amplified from p*RPS5A*::TMO5:GR template (*1*) and combined using LIC (*59*). p*RPS5A*::CKX3 line was generated by cloning the CDS into pPLV28 using LIC. p*SHR*::nYFP was generated by cloning the promoter fragment (*60*) together with nYFP into pH7m34GW destination vector using Gateway cloning. p*SHR*::TMO5:GR by combining *SHR* promoter fragment, *TMO5* CDS and GR tag into pH7m34GW, using Gateway cloning. p*WOL*::XVE>>TMO5:YFP and p*WOL*::XVE>>LOG4:YFP were generated by subcloing the respective CDS with pDONRP4p1r-pWOL-XVE (*60*) and YFP into pH7m34GW using Gateway cloning. All constructs were verified by Sanger sequencing and were transformed into wild type using simplified floral dipping (*61*). All primer sequences used for cloning and sequencing can be found in **Table S3**.

Plant imaging, image processing and data analysis

Marker lines and different genotypes were either fixed with ClearSee, stained with Calcofluor White and mounted on sides with ClearSee solution (*62*) or directly mounted on slides containing 0.1 mg/ml propidium iodide (PI) for cell wall staining. Confocal microscopy on marker lines was performed on a Leica SP8X using a 40x lens (water corrected objective lens with NA 1.2). For 3-dimensional (3D) imaging and segmentation analysis, 6-das wild type roots were stained using the modified pseudo-Schiff-PI (mPS-PI) staining method (*63*). 3D segmentation of the primary root meristem was performed on 3D z-stacks using the MorphoGraphX software (*64*) and cell numbers per cell type were scored in two individual roots (averages used in plot). For root hair analysis, 10-day-old seedling roots were imaged on the plate with a Leica stereomicroscope at 32x magnification. Additionally, confocal imaging was applied to generate a 3D stack of a full one mm of mature primary root on a Leica SP8X using a 10x dry-lens on samples fixed with ClearSee and stained with Calcofluor White. This stack was generated by imaging in XZY-direction, taking 150 images at ~6.7 µm intervals. For a description of the phenotypic parameters that were measured, see **Fig. S16** and the materials and methods phenotyping section below. Calcofluor White, GFP, YFP, tdTomato and PI samples were imaged at an excitation of 405nm, 488nm, 514nm, 561nm and 514nm respectively. Calcofluor White, GFP, YFP, tdTomato and PI were visualized at an emission of 425-475 nm, 500-535nm, 520-550nm, 580-630nm and 600-700nm respectively. GUS staining was performed as described previously (*65*). For esthetic reasons, some sets of images were globally adjusted in brightness and contrast, rotated, and displayed on a matching background. Plots were generated using R package "ggplot2" (*66*). In all boxplots, boxes represent the 1st and 3rd quartile and the center line represents the median. Data point-shapes represent biological replicates and number of measurements are shown above the x-

axis. Statistical analyses were performed using either One-way-ANOVA or Chi-square tests and p-values below 0.001 were considered significant, unless otherwise stated. All figures were compiled using Adobe Illustrator.

Phenotyping

The approaches used for analysis of the range of phenotypic parameters described in **Fig. S16** are explained below in more detail. From scanned plates, total primary root lengths were measured using Fiji software. From stereomicroscope images, both the number of root hairs in 1 mm of root and the root hair lengths were measured in the maturation zone of the primary root using Fiji software. From 3D-confocal stacks, the number of cortex and number of epidermal cells (hair vs non-hair position) were counted in one representative cross-section. Additionally, the total number of hairs and the number of cells in non-hair position that form root hairs were counted along the full stack. Similar imaging and phenotyping was performed on p*COBL9*::GFP (hair marker) and p*GL2*::GFP (non-hair marker) lines. Here, the number of cells, ectopically expressing the marker, were counted along the entire stack. Meristem length was determined from longitudinal confocal sections of the primary root and measured as the distance from quiescent center to the first elongated cortical cell. Epidermal cell length was determined by measuring the length of ten trichoblast cells on a longitudinal confocal section from the same 1 mm region of the root where root hairs were counted. A summary of all phenotypic measurements related to cell numbers and root hairs, on respective genotypes and treatments is presented in **Table S2**.

Relative expression analysis

Total RNA was isolated using an RNeasy kit (QIAGEN). cDNA was synthesized using 1 µg of total RNA and a qScript cDNA SuperMix (QUANTABIO) and manufacturer's instructions. Relative expression was measured in triplicate by Q-RT-PCR on a LightCycler480 II apparatus (Roche) with SYBR GREEN I Master kit (Roche) and manufacturer's instructions. Data were analyzed using qBase+ software package (Biogazelle). Expression levels were normalized to those of EEF1a4 and UBC21. All primers used for Q-RT-PCR analysis can be found in **Table S3**.

References

1. B. De Rybel *et al.*, Plant development. Integration of growth and patterning during vascular tissue formation in Arabidopsis. *Science* **345**, 1255215 (2014).
2. B. De Rybel *et al.*, A bHLH complex controls embryonic vascular tissue establishment and indeterminate growth in Arabidopsis. *Dev Cell* **24**, 426-437 (2013).
3. K. Ohashi-Ito, D. C. Bergmann, Regulation of the Arabidopsis root vascular initial population by LONESOME HIGHWAY. *Development* **134**, 2959-2968 (2007).
4. K. Ohashi-Ito, M. Matsukawa, H. Fukuda, An atypical bHLH transcription factor regulates early xylem development downstream of auxin. *Plant Cell Physiol* **54**, 398-405 (2013).
5. K. Ohashi-Ito, M. Oguchi, M. Kojima, H. Sakakibara, H. Fukuda, Auxin-associated initiation of vascular cell differentiation by LONESOME HIGHWAY. *Development* **140**, 765-769 (2013).
6. K. Ohashi-Ito *et al.*, A bHLH complex activates vascular cell division via cytokinin action in root apical meristem. *Curr Biol* **24**, 2053-2058 (2014).
7. F. Vera-Sirera *et al.*, A bHLH-Based Feedback Loop Restricts Vascular Cell Proliferation in Plants. *Dev Cell* **35**, 432-443 (2015).
8. T. Kuroha *et al.*, Functional analyses of LONELY GUY cytokinin-activating enzymes reveal the importance of the direct activation pathway in Arabidopsis. *The Plant Cell* **21**, 3152-3169 (2009).
9. H. Tokunaga *et al.*, Arabidopsis lonely guy (LOG) multiple mutants reveal a central role of the LOG-dependent pathway in cytokinin activation. *The Plant journal* **69**, 355-365 (2012).
10. S. Miyashima *et al.*, Mobile PEAR transcription factors integrate positional cues to prime cambial growth. *Nature* **565**, 490-494 (2019).
11. W. Smet *et al.*, DOF2.1 Controls Cytokinin-Dependent Vascular Cell Proliferation Downstream of TMO5/LHW. *Current biology : CB* **29**, 520-529 e526 (2019).
12. K. Jean-Baptiste *et al.*, Dynamics of Gene Expression in Single Root Cells of Arabidopsis. *Plant Cell* **31**, 993-1011 (2019).
13. T. Denyer *et al.*, Spatiotemporal Developmental Trajectories in the Arabidopsis Root Revealed Using High-Throughput Single-Cell RNA Sequencing. *Dev Cell* **48**, 840-852.e845 (2019).
14. T. Q. Zhang, Z. G. Xu, G. D. Shang, J. W. Wang, A Single-Cell RNA Sequencing Profiles the Developmental Landscape of Arabidopsis Root. *Mol Plant* **12**, 648-660 (2019).
15. K. H. Ryu, L. Huang, H. M. Kang, J. Schiefelbein, Single-Cell RNA Sequencing Resolves Molecular Relationships Among Individual Plant Cells. *Plant Physiol* **179**, 1444-1456 (2019).
16. C. N. Shulse *et al.*, High-Throughput Single-Cell Transcriptome Profiling of Plant Cell Types. *Cell Rep* **27**, 2241-2247.e2244 (2019).
17. S. Li, M. Yamada, X. Han, U. Ohler, P. N. Benfey, High-Resolution Expression Map of the Arabidopsis Root Reveals Alternative Splicing and lincRNA Regulation. *Dev Cell* **39**, 508-522 (2016).
18. R. Ruonala, D. Ko, Y. Helariutta, Genetic Networks in Plant Vascular Development. *Annu Rev Genet* **51**, 335-359 (2017).
19. A. Rodriguez-Villalon *et al.*, Molecular genetic framework for protophloem formation. *Proc Natl Acad Sci U S A* **111**, 11551-11556 (2014).
20. A. P. Mähönen *et al.*, A novel two-component hybrid molecule regulates vascular morphogenesis of the Arabidopsis root. *Genes & development* **14**, 2938-2943 (2000).

21. R. Bhosale *et al.*, A Spatiotemporal DNA Endoploidy Map of the Arabidopsis Root Reveals Roles for the Endocycle in Root Development and Stress Adaptation. *Plant Cell* **30**, 2330-2351 (2018).
22. R. Bhosale *et al.*, A mechanistic framework for auxin dependent Arabidopsis root hair elongation to low external phosphate. *Nat Commun* **9**, 1409 (2018).
23. J. E. Salazar-Henao, I. C. Vélez-Bermúdez, W. Schmidt, The regulation and plasticity of root hair patterning and morphogenesis. *Development* **143**, 1848-1858 (2016).
24. M. Grebe *et al.*, Cell polarity signaling in Arabidopsis involves a BFA-sensitive auxin influx pathway. *Curr Biol* **12**, 329-334 (2002).
25. H. Rouached, A. B. Arpat, Y. Poirier, Regulation of phosphate starvation responses in plants: signaling players and cross-talks. *Mol Plant* **3**, 288-299 (2010).
26. Z. H. Chen, G. A. Nimmo, G. I. Jenkins, H. G. Nimmo, BHLH32 modulates several biochemical and morphological processes that respond to Pi starvation in Arabidopsis. *Biochem J* **405**, 191-198 (2007).
27. Z. Ma, D. G. Bielenberg, K. M. Brown, J. P. Lynch, Regulation of root hair density by phosphorus availability in *Arabidopsis thaliana*. *Plant Cell and Environment* **24**, 459-467 (2001).
28. A. Schlereth *et al.*, MONOPTEROS controls embryonic root initiation by regulating a mobile transcription factor. *Nature* **464**, 913-916 (2010).
29. P. Wu *et al.*, Phosphate starvation triggers distinct alterations of genome expression in Arabidopsis roots and leaves. *Plant Physiol* **132**, 1260-1271 (2003).
30. E. Zurcher *et al.*, A robust and sensitive synthetic sensor to monitor the transcriptional output of the cytokinin signaling network in planta. *Plant Physiology* **161**, 1066-1075 (2013).
31. K. C. Potter, J. Wang, G. E. Schaller, J. J. Kieber, Cytokinin modulates context-dependent chromatin accessibility through the type-B response regulators. *Nat Plants* **4**, 1102-1111 (2018).
32. I. H. Street *et al.*, Cytokinin acts through the auxin influx carrier AUX1 to regulate cell elongation in the root. *Development* **143**, 3982-3993 (2016).
33. L. Song *et al.*, The Molecular Mechanism of Ethylene-Mediated Root Hair Development Induced by Phosphate Starvation. *PLoS Genet* **12**, e1006194 (2016).
34. S. Zhang *et al.*, Multiple phytohormones promote root hair elongation by regulating a similar set of genes in the root epidermis in Arabidopsis. *J Exp Bot* **67**, 6363-6372 (2016).
35. T. Schmülling, T. Werner, M. Riefler, E. Krupková, I. Bartrina y Manns, Structure and function of cytokinin oxidase/dehydrogenase genes of maize, rice, Arabidopsis and other species. *J Plant Res* **116**, 241-252 (2003).
36. G. Janes *et al.*, Cellular Patterning of Arabidopsis Roots Under Low Phosphate Conditions. *Front Plant Sci* **9**, 735 (2018).
37. S. M. Brady, S. Song, K. S. Dhugga, J. A. Rafalski, P. N. Benfey, Combining expression and comparative evolutionary analysis. The COBRA gene family. *Plant Physiol* **143**, 172-187 (2007).
38. Y. Lin, J. Schiefelbein, Embryonic control of epidermal cell patterning in the root and hypocotyl of Arabidopsis. *Development* **128**, 3697-3705 (2001).
39. M. Simon, M. M. Lee, Y. Lin, L. Gish, J. Schiefelbein, Distinct and overlapping roles of single-repeat MYB genes in root epidermal patterning. *Dev Biol* **311**, 566-578 (2007).
40. M. Bonke, S. Thitamadee, A. P. Mahonen, M. T. Hauser, Y. Helariutta, APL regulates vascular tissue identity in Arabidopsis. *Nature* **426**, 181-186 (2003).

41. J. M. Alonso, T. Hirayama, G. Roman, S. Nourizadeh, J. R. Ecker, EIN2, a bifunctional transducer of ethylene and stress responses in Arabidopsis. *Science* **284**, 2148-2152 (1999).
42. T. Potuschak *et al.*, EIN3-dependent regulation of plant ethylene hormone signaling by two arabidopsis F box proteins: EBF1 and EBF2. *Cell* **115**, 679-689 (2003).
43. M. K. Zhiponova *et al.*, Helix-loop-helix/basic helix-loop-helix transcription factor network represses cell elongation in Arabidopsis through an apparent incoherent feed-forward loop. *Proc Natl Acad Sci U S A* **111**, 2824-2829 (2014).
44. J. Goossens, G. Swinnen, R. Vanden Bossche, L. Pauwels, A. Goossens, Change of a conserved amino acid in the MYC2 and MYC3 transcription factors leads to release of JAZ repression and increased activity. *New Phytol* **206**, 1229-1237 (2015).
45. A. Coego *et al.*, The TRANSPLANTA collection of Arabidopsis lines: a resource for functional analysis of transcription factors based on their conditional overexpression. *Plant J* **77**, 944-953 (2014).
46. A. S. Iyer-Pascuzzi, P. N. Benfey, Fluorescence-activated cell sorting in plant developmental biology. *Methods Mol Biol* **655**, 313-319 (2010).
47. A. T. Lun, K. Bach, J. C. Marioni, Pooling across cells to normalize single-cell RNA sequencing data with many zero counts. *Genome Biol* **17**, 75 (2016).
48. A. T. Lun, D. J. McCarthy, J. C. Marioni, A step-by-step workflow for low-level analysis of single-cell RNA-seq data with Bioconductor. *F1000Res* **5**, 2122 (2016).
49. C. S. McGinnis, L. M. Murrow, Z. J. Gartner, DoubletFinder: Doublet Detection in Single-Cell RNA Sequencing Data Using Artificial Nearest Neighbors. *Cell Syst* **8**, 329-337.e324 (2019).
50. K. Birnbaum *et al.*, A gene expression map of the Arabidopsis root. *Science (New York, N.Y* **302**, 1956-1960 (2003).
51. W. Saelens, R. Cannoodt, H. Todorov, Y. Saeys, A comparison of single-cell trajectory inference methods. *Nat Biotechnol* **37**, 547-554 (2019).
52. K. Street *et al.*, Slingshot: cell lineage and pseudotime inference for single-cell transcriptomics. *BMC Genomics* **19**, 477 (2018).
53. L. Muñiz *et al.*, ACAULIS5 controls Arabidopsis xylem specification through the prevention of premature cell death. *Development* **135**, 2573-2582 (2008).
54. A. Carlsbecker *et al.*, Cell signalling by microRNA165/6 directs gene dose-dependent root cell fate. *Nature* **465**, 316-321 (2010).
55. M. Kubo *et al.*, Transcription switches for protoxylem and metaxylem vessel formation. *Genes Dev* **19**, 1855-1860 (2005).
56. M. Taylor-Teeples *et al.*, An Arabidopsis gene regulatory network for secondary cell wall synthesis. *Nature* **517**, 571-575 (2015).
57. S. Otero, Y. Helariutta, Companion cells: a diamond in the rough. *J Exp Bot* **68**, 71-78 (2017).
58. V. López-Salmerón, H. Cho, N. Tonn, T. Greb, The Phloem as a Mediator of Plant Growth Plasticity. *Curr Biol* **29**, R173-R181 (2019).
59. J. R. Wendrich, C. Y. Liao, W. A. van den Berg, B. De Rybel, D. Weijers, Ligation-independent cloning for plant research. *Methods Mol Biol* **1284**, 421-431 (2015).
60. R. Siligato *et al.*, MultiSite Gateway-Compatible Cell Type-Specific Gene-Inducible System for Plants. *Plant Physiol* **170**, 627-641 (2016).
61. S. J. Clough, A. F. Bent, Floral dip: a simplified method for Agrobacterium-mediated transformation of Arabidopsis thaliana. *Plant Journal* **16**, 735-743 (1998).
62. R. Ursache, T. G. Andersen, P. Marhavý, N. Geldner, A protocol for combining fluorescent proteins with histological stains for diverse cell wall components. *Plant J* **93**, 399-412 (2018).

63. E. Truernit *et al.*, High-resolution whole-mount imaging of three-dimensional tissue organization and gene expression enables the study of Phloem development and structure in Arabidopsis. *The Plant Cell* **20**, 1494-1503 (2008).
64. P. Barbier de Reuille *et al.*, MorphoGraphX: A platform for quantifying morphogenesis in 4D. *Elife* **4**, 05864 (2015).
65. B. De Rybel *et al.*, A novel Aux/IAA28 signaling cascade activates GATA23-dependent specification of lateral root founder cell identity. *Current biology* **20**, 1697-1706 (2010).
66. H. Wickham, *ggplot2, Elegant Graphics for Data Analysis*. Use R! (Springer-Verlag New York, 2009), vol. 1, pp. VIII, 213.

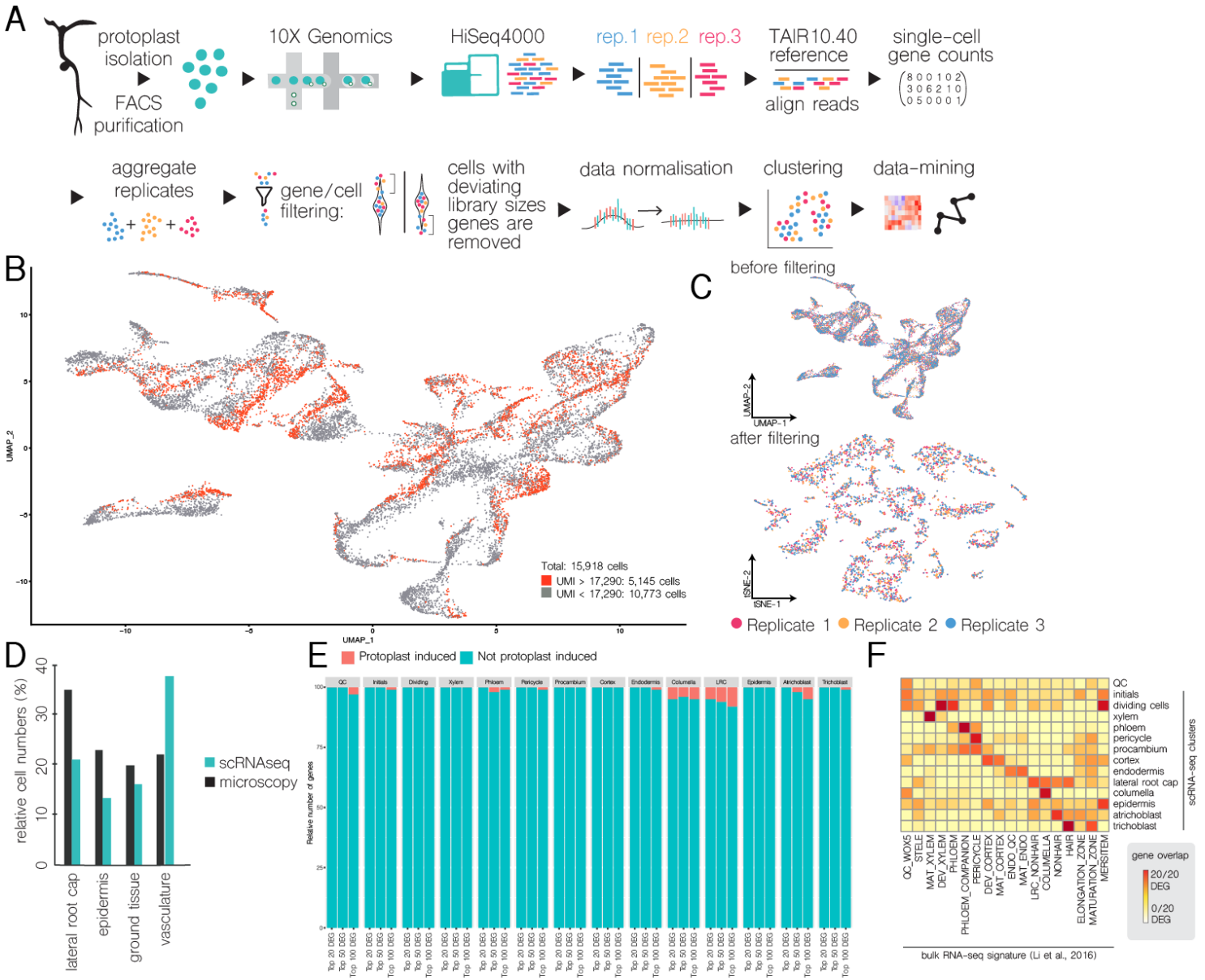
A
protoplast isolation
FACS purification
10X Genomics
HiSeq4000
rep.1 rep.2 rep.3
TAIR10.40 reference
align reads
single-cell gene counts
aggregate replicates
gene/cell filtering:
cells with deviating library sizes genes are removed
data normalisation
clustering
data-mining
B
UMAP_1
UMAP_2
Total: 15,918 cells
UMI > 17,290: 5,145 cells
UMI < 17,290: 10,773 cells
C
before filtering
after filtering
UMAP-1
UMAP-2
tSNE-1
tSNE-2
Replicate 1
Replicate 2
Replicate 3
D
relative cell numbers (%)
scRNAseq
microscopy
lateral root cap
epidermis
ground tissue
vasculature
E
Protoplast induced
Not protoplast induced
Relative number of genes
QC
Initials
Dividing
Xylem
Phloem
Pericycle
Procambium
Cortex
Endodermis
Columella
LRC
Epidermis
Atrichoblast
Trichoblast
Top 20 DEG
Top 50 DEG
Top 100 DEG
F
QC
initials
dividing cells
xylem
phloem
pericycle
procambium
cortex
endodermis
lateral root cap
columella
epidermis
atrichoblast
trichoblast
scRNA-seq clusters
QC_WOX5
STELE
MAT_XYLEM
DEV_XYLEM
PHLOEM
PHLOEM_COMPANION
PERICYCLE
DEV_CORTEX
MAT_CORTEX
ENDO_QC
MAT_ENDO
LRC_NONHAIR
COLUMELLA
NONHAIR
HAIR
ELONGATION_ZONE
MATURATION_ZONE
MERISTEM
bulk RNA-seq signature (Li et al., 2016)
gene overlap
20/20 DEG
0/20 DEG

Fig. S1. Pipeline and quality control of the single cell dataset. A. Overview of the scRNA-seq pipeline, including metrics of the scRNA-seq experiment. **B.** UMAP projection of all recovered cells (gene count > 200) from the single cell RNAseq dataset. High quality cells with UMI count > 17,290 are indicated in red, the other cells in grey. **C.** Color-coded UMAP and tSNE plot (before and after UMI filtering, respectively) depicting three replicate experiments, contributing to all clusters to assess for batch effects and reproducibility. **D.** Comparison of the number of cells in each identity cluster with the actual number of cells quantified using 3D confocal microscopy and segmentation analysis. **E.** Contribution of genes induced by protoplasting to cell identity clusters. Bar chart showing the prevalence of genes induced by protoplasting (*50*) in different cell identity clusters. **F.** Comparison of the scRNA-seq dataset to previously published cell type-specific bulk RNAseq (*17*).

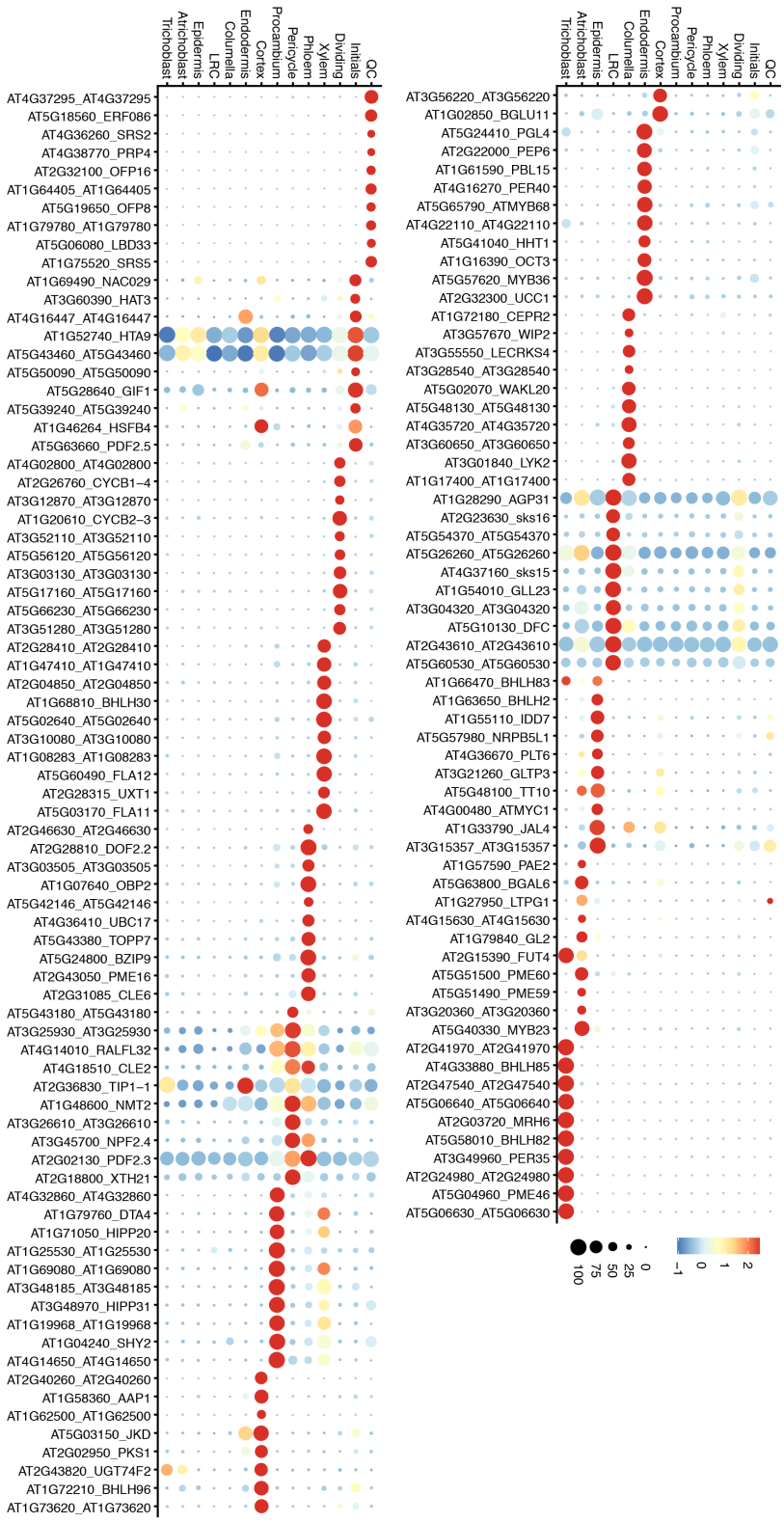

Fig. S2. Identification of tissue specific reporter genes. Dot-plot of identified tissue specific genes for each cell identity, containing known and uncharacterized genes. Size of the circles represents the percentage of cells with expression (pct.exp.), while the color indicates the scaled average expression level of this gene in each cell type (avg exp. scale).

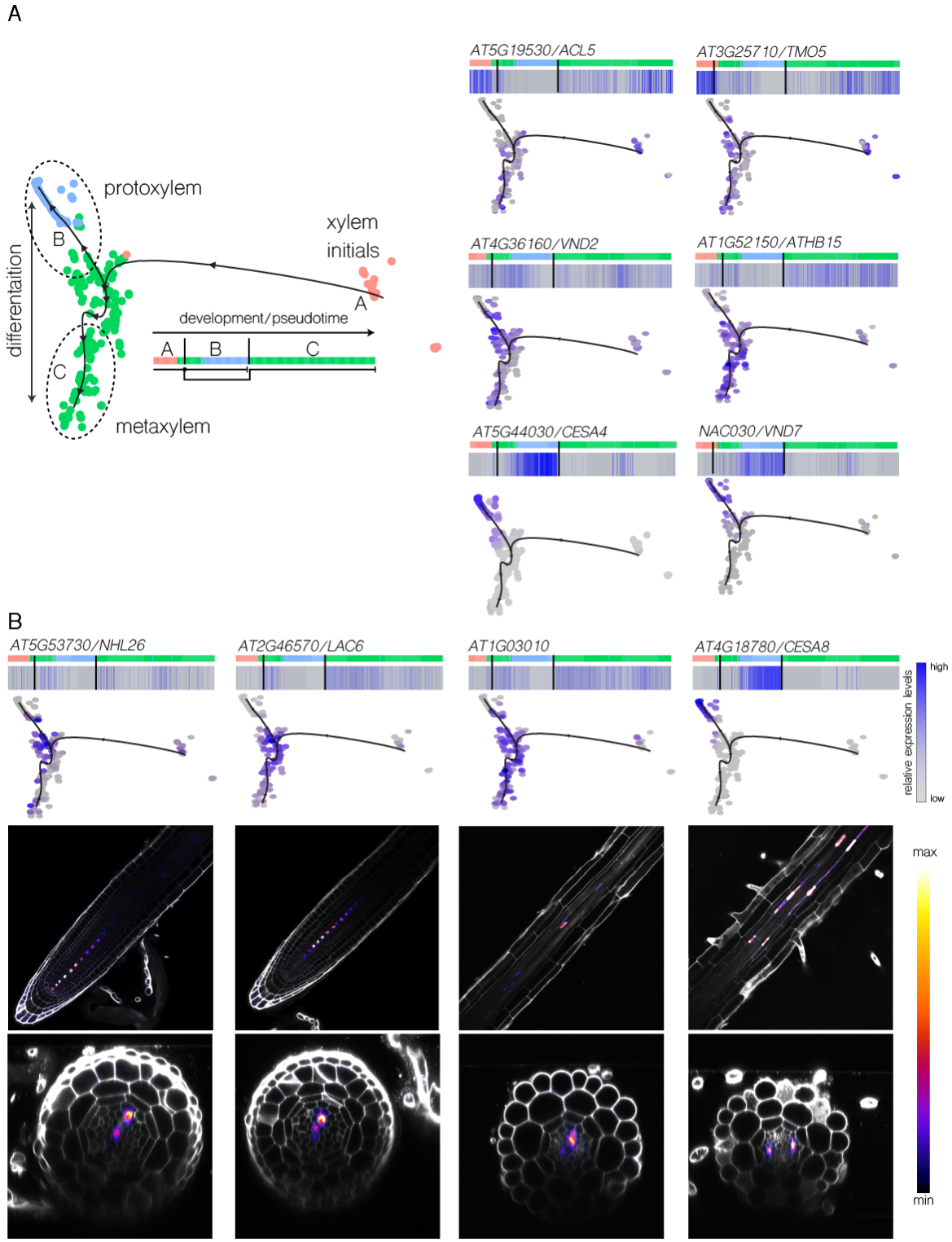

Fig. S3. Trajectory analysis and validation for the xylem cluster. A. Predicted developmental trajectory of xylem cluster cells starting from xylem initials (A, red) and branching into protoxylem (B, green and blue) and metaxylem (C, green) trajectories (left side). Validation of the predicted trajectory using known developmental regulators for the xylem, including the heatmap and feature plots (right side). **B.** Experimental validation of xylem trajectory including the heatmaps, feature plots and reporter line expression patterns of predicted xylem (specific) expressed genes.

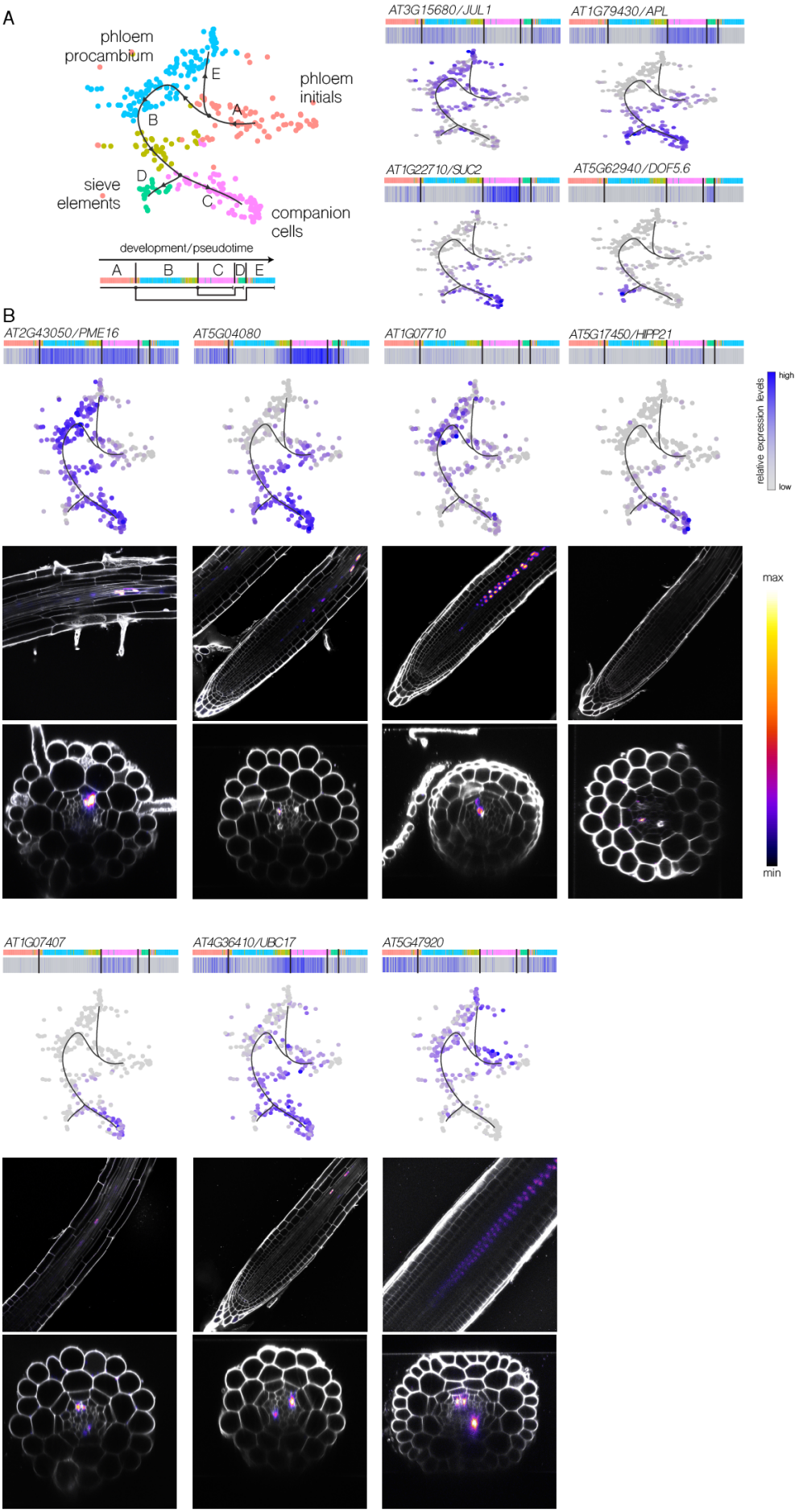
A
phloem
procambium
phloem
initials
sieve
elements
companion
cells
E
A
B
D
C
development/pseudotime
A
B
C
D
E
AT3G15680/JUL1
AT1G79430/APL
AT1G22710/SUC2
AT5G62940/DOF5.6
B
AT2G43050/PME16
AT5G04080
AT1G07710
AT5G17450/HIPP21
high
relative expression levels
low
max
min
AT1G07407
AT4G36410/UBC17
AT5G47920

Fig. S4. Trajectory analysis and validation for the phloem cluster. A. Predicted developmental trajectory of phloem cluster cells starting from phloem initials (A, red) first branching off into phloem procambium (PC) (E, blue) and next branching into sieve elements (SE) (D, green) and companion cells (CC) (C, pink) trajectories (left side). Validation of the predicted trajectory using known developmental regulators for the phloem, including heatmaps and feature plots (right). **B.** Experimental validation of phloem trajectory including the heatmaps, feature plots and reporter line expression patterns of predicted phloem (specific) expressed genes.

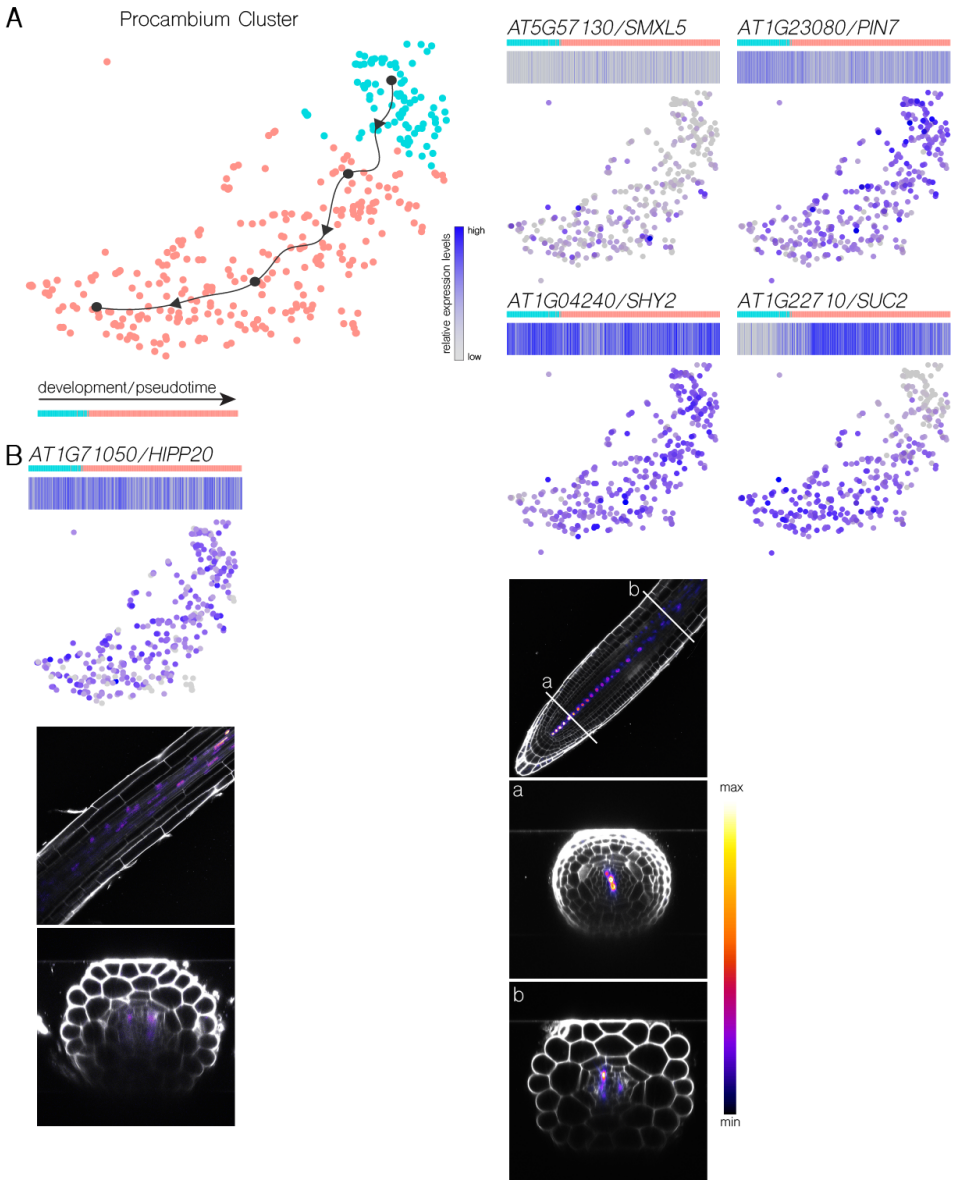

Fig. S5. Trajectory analysis and validation for the procambium cluster. A. Predicted developmental trajectory of the procambium cluster cells putatively going from the initials to the more differentiated cells (left side). Validation of the predicted trajectory using the limited known developmental regulators for the procambium, including the heatmap and feature plots (right). **B.** Experimental validation of procambium trajectory including heatmap, feature plot and reporter line expression pattern of a predicted procambium expressed gene, *AT1G71050/HIPP20*.

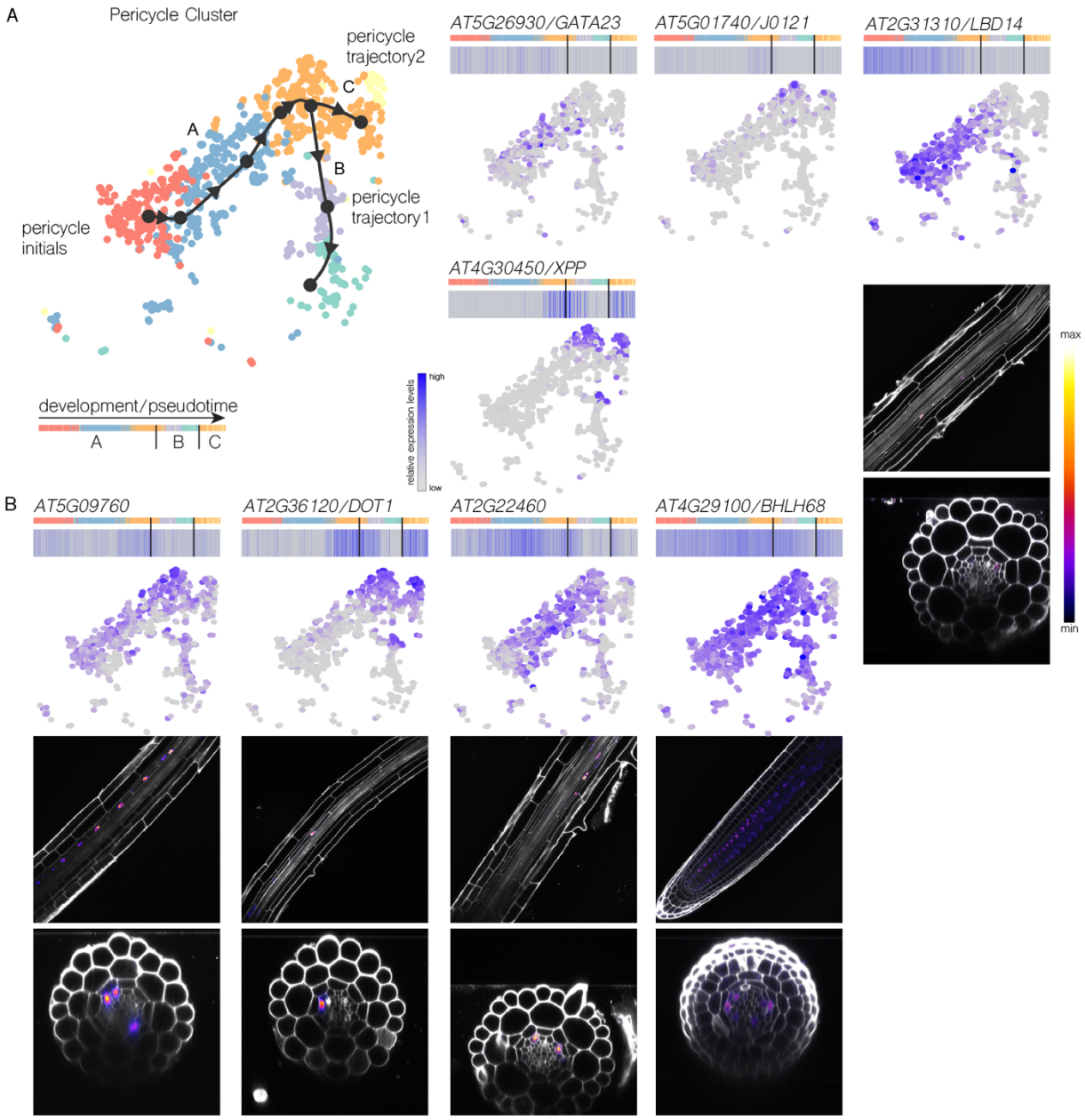

Fig. S6. Trajectory analysis and validation for the pericycle cluster. A. Predicted developmental trajectory of the pericycle cluster cells going from the initials to the more differentiated cells. Note the bifurcation into two distinct trajectories (left side). Validation of the predicted trajectory using known developmental regulators for the pericycle, including heatmaps and feature plots (right). **B.** Experimental validation of pericycle trajectory including the heatmaps, feature plots and reporter line expression patterns of predicted pericycle (specific) expressed genes.

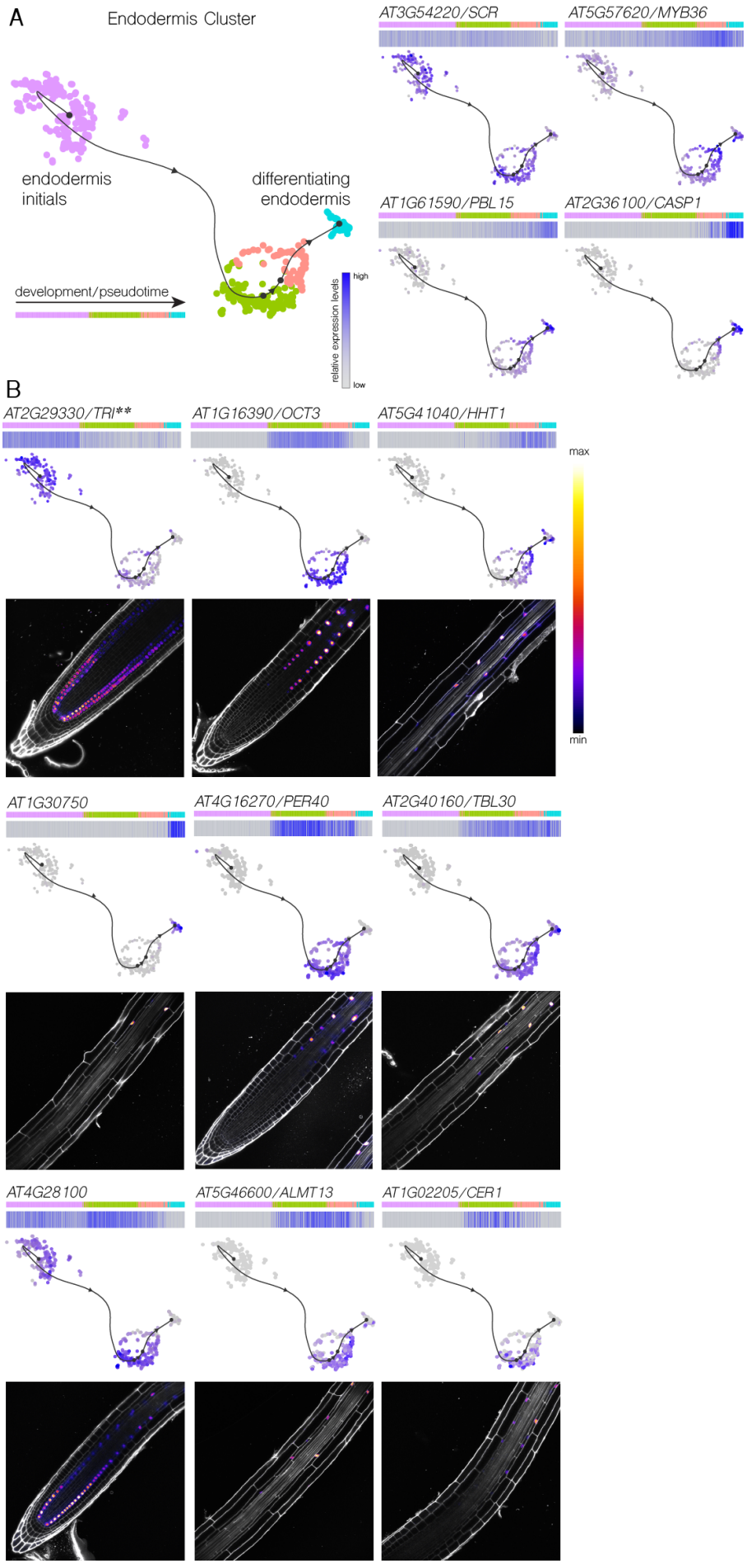
A
Endodermis Cluster
endodermis initials
differentiating endodermis
development/pseudotime
relative expression levels
high
low
AT3G54220/SCR
AT5G57620/MYB36
AT1G61590/PBL15
AT2G36100/CASP1
B
AT2G29330/TRI**
AT1G16390/OCT3
AT5G41040/HHT1
max
min
AT1G30750
AT4G16270/PER40
AT2G40160/TBL30
AT4G28100
AT5G46600/ALMT13
AT1G02205/CER1

Fig. S7. Trajectory analysis and validation for the endodermis cluster. A. Predicted developmental trajectory of the endodermis cluster cells going from the initials to the more differentiated cells (left side). Validation of the predicted trajectory using known developmental regulators for the endodermis, including the heatmap and feature plots (right). **B.** Experimental validation of endodermis trajectory including the heatmaps, feature plots and reporter line expression patterns of predicted endodermis (specific) expressed genes. **: this gene is expressed in both endodermis and cortex and is used as validation for both trajectories (see also Fig. S8.)

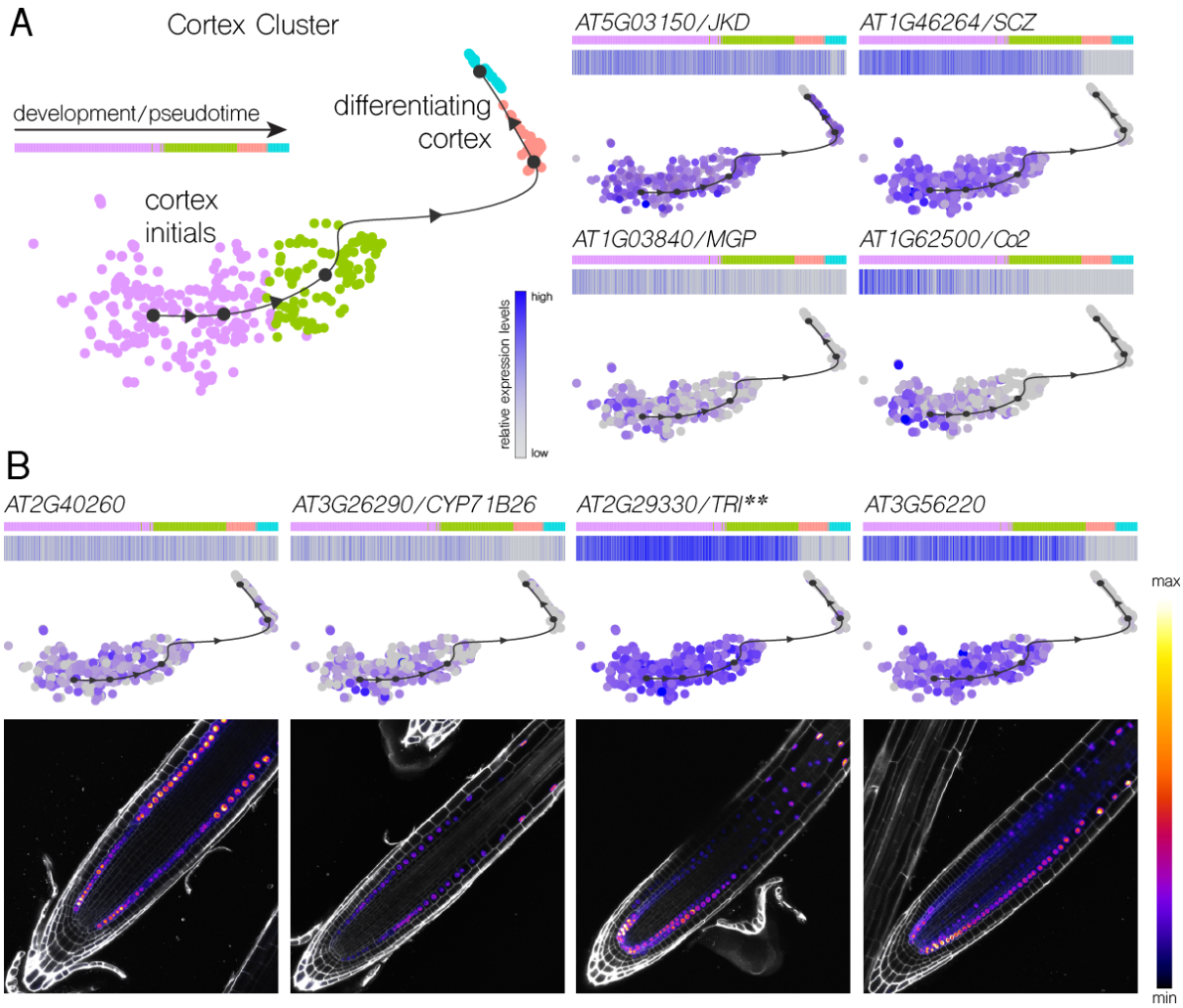

Fig. S8. Trajectory analysis and validation for the cortex cluster. A. Predicted developmental trajectory of the cortex cluster cells going from the initials to the more differentiated cells (left side). Validation of the predicted trajectory using known developmental regulators for the cortex, including the heatmap and feature plots (right). **B.** Experimental validation of cortex trajectory including the heatmaps, feature plots and reporter line expression patterns of predicted cortex (specific) expressed genes. **: this gene is expressed in both endodermis and cortex and is used as validation for both trajectories (see also Fig. S7.)

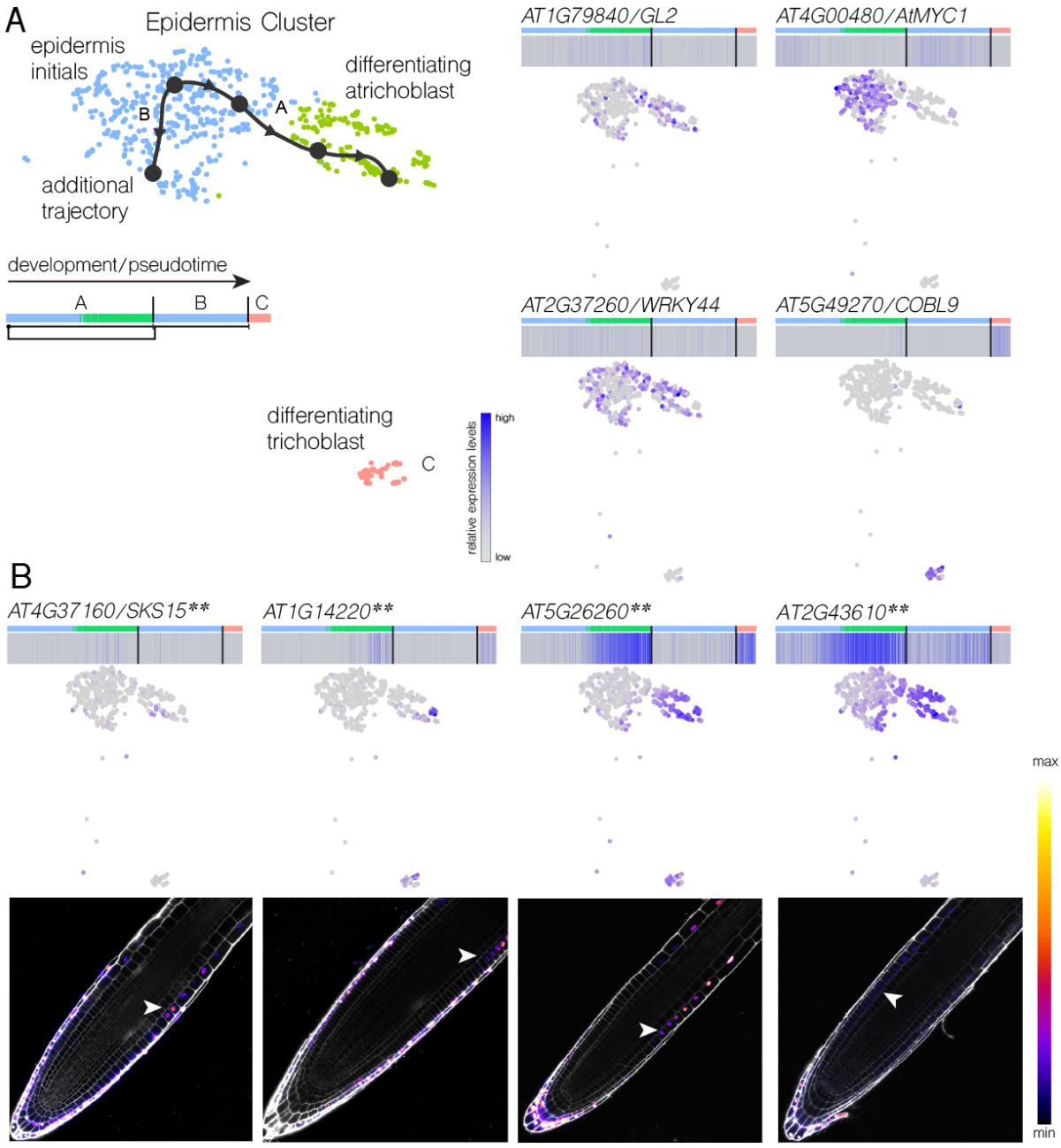

Fig. S9. Trajectory analysis and validation for the epidermis cluster. A. Predicted developmental trajectory of the epidermis cluster cells going from the initials to the more differentiated cells. Note the bifurcation into two distinct trajectories (left side). Validation of the predicted trajectory using known developmental regulators for the epidermis, including the heatmap and feature plots (right). **B.** Experimental validation of epidermis trajectory including the heatmaps, feature plots and reporter line expression patterns of predicted epidermis expressed genes. **: these genes are expressed in both epidermis and lateral root cap and are used as validation for both trajectories (see also Fig. S10).

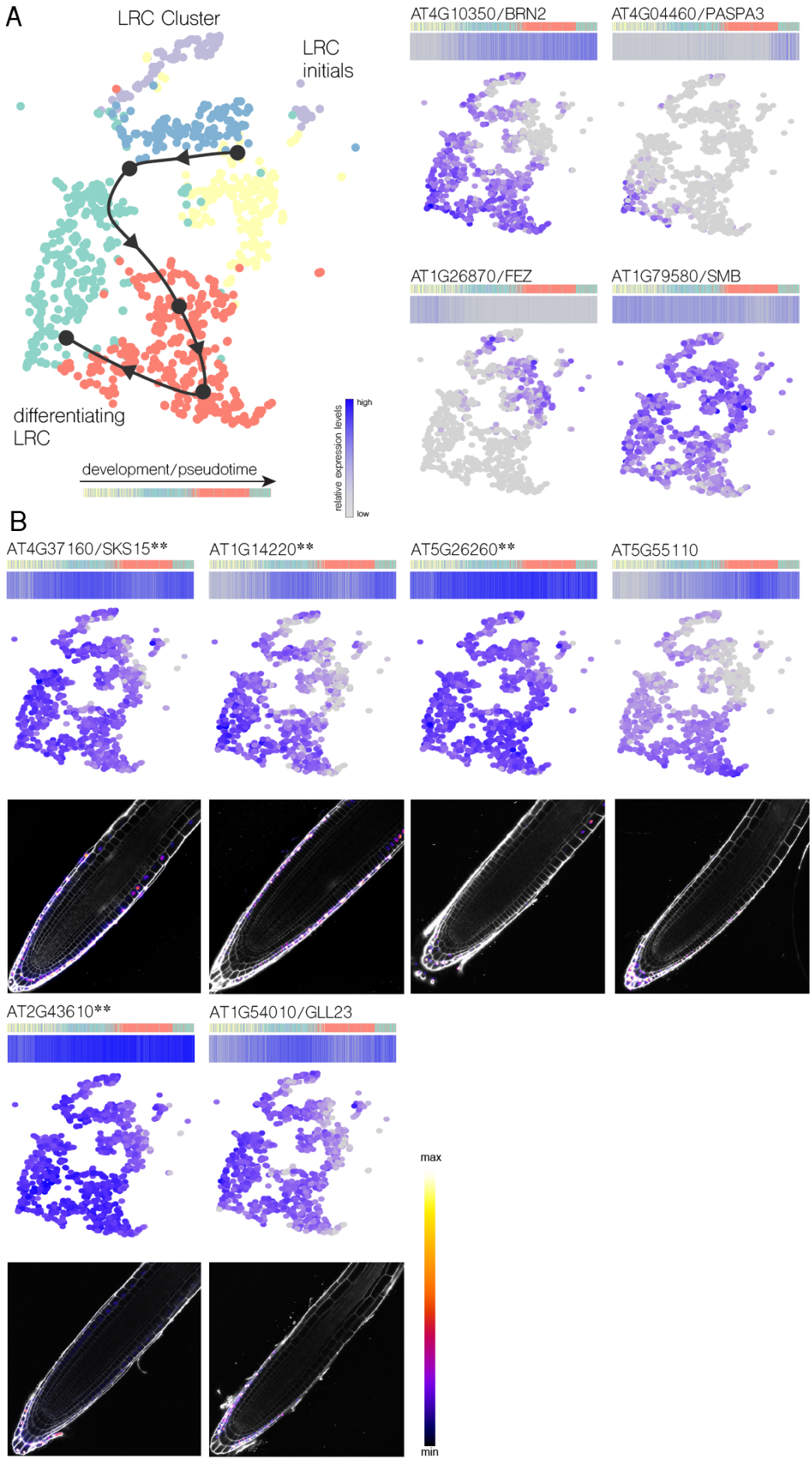
A
LRC Cluster
LRC initials
differentiating LRC
development/pseudotime
relative expression levels
high
low
AT4G10350/BRN2
AT4G04460/PASPA3
AT1G26870/FEZ
AT1G79580/SMB
B
AT4G37160/SKS15**
AT1G14220**
AT5G26260**
AT5G55110
AT2G43610**
AT1G54010/GLL23
max
min

Fig. S10. Trajectory analysis and validation for the lateral root cap (LRC) cluster. A. Predicted developmental trajectory of the LRC cluster cells going from the initials to the more differentiated cells (left side). Validation of the predicted trajectory using known developmental regulators for the LRC, including the heatmap and feature plots (right). **B.** Experimental validation of LRC trajectory including the heatmaps, feature plots and reporter line expression patterns of predicted LRC (specific) expressed genes. **: these genes are expressed in both lateral root cap and epidermis and are used as validation for both trajectories (see also Fig. S9).

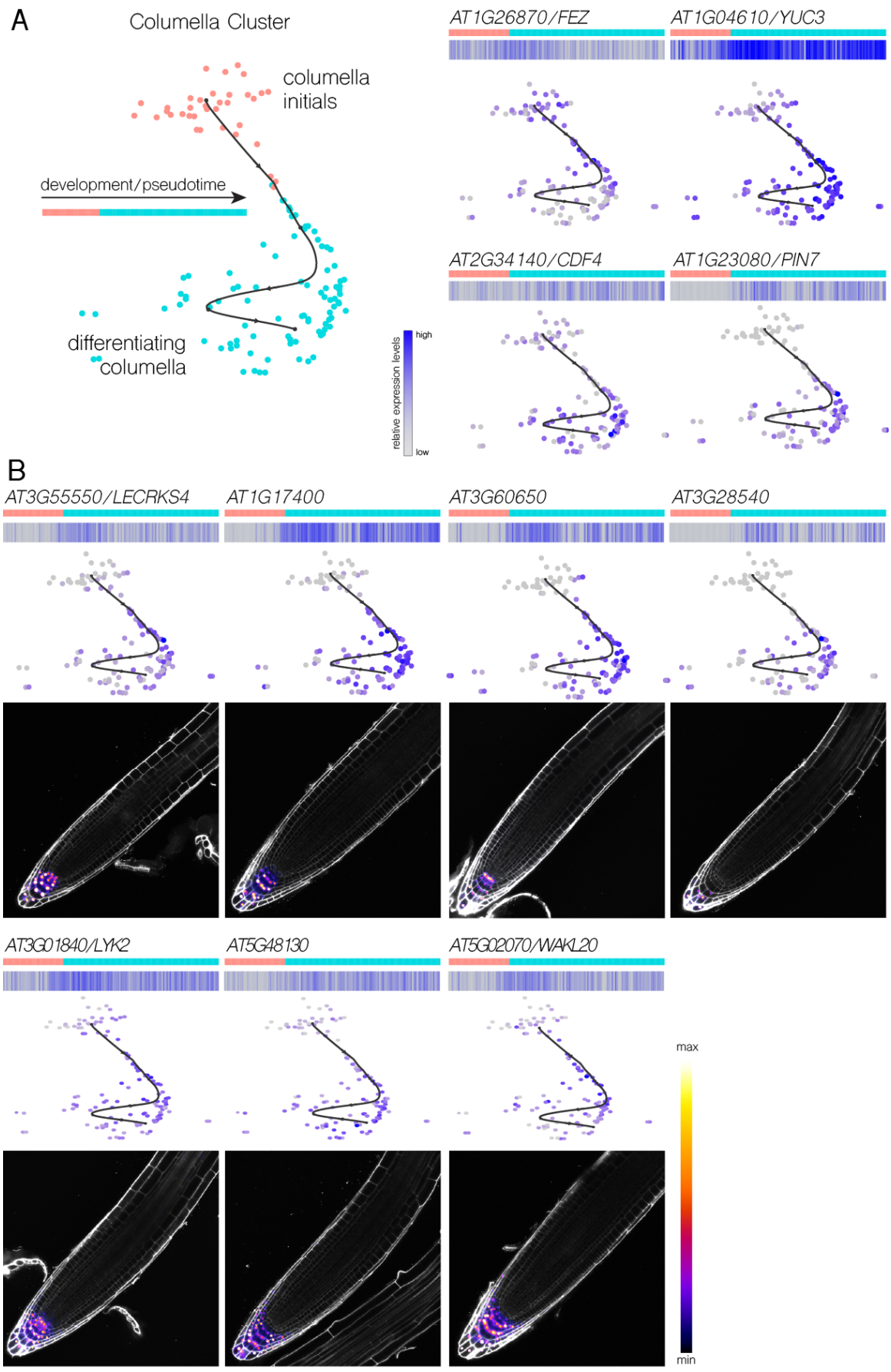
A
Columella Cluster
columella initials
development/pseudotime
differentiating columella
relative expression levels
high
low
AT1G26870/FEZ
AT1G04610/YUC3
AT2G34140/CDF4
AT1G23080/PIN7
B
AT3G55550/LECRKS4
AT1G17400
AT3G60650
AT3G28540
AT3G01840/LYK2
AT5G48130
AT5G02070/WAKL20
max
min

Fig. S11. Trajectory analysis and validation for the columella cluster. A. Predicted developmental trajectory of the columella cluster cells going from the initials to the more differentiated cells. Validation of the predicted trajectory using known developmental regulators for the columella, including the heatmap and feature plots (right). **B.** Experimental validation of columella trajectory including the heatmaps, feature plots and reporter line expression patterns of predicted columella (specific) expressed genes.

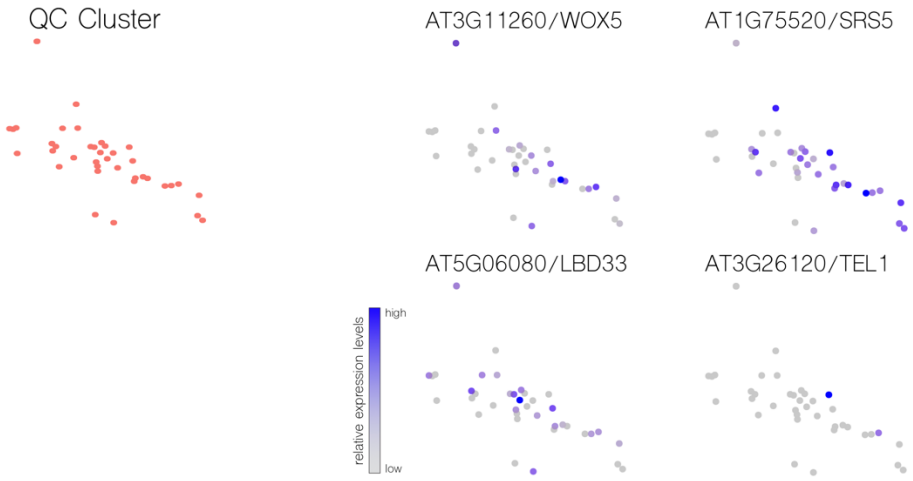

Fig. S12. Validation for the quiescent center (QC) cluster. Validation of the predicted QC cluster (left) using limited known developmental regulators for the QC, including feature plots (right).

Fig. S13. Tissue specific expression of TMO5/LHW targets. Dot-plot of the tissue specific expression of the 273 putative TMO5/LHW target genes illustrating the large number of trichoblast expressed genes. Size of the circles represents the percentage of cells with expression (pct.exp.), while the color indicates the scaled average expression level of this gene in each cell type (avg exp. scale).

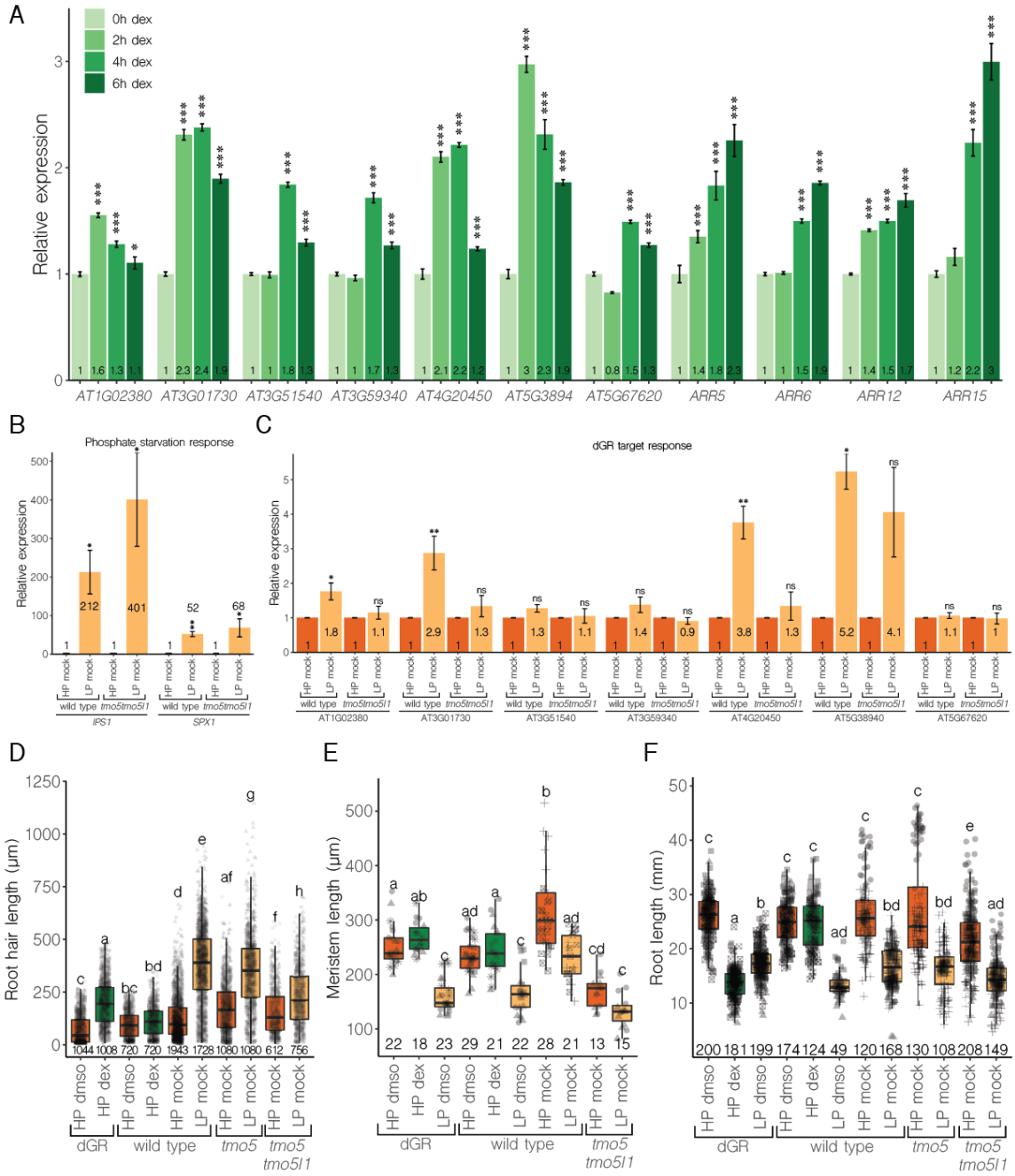

Fig. S14. A-C. Relative expression analyses using Q-RT-PCR. **A.** Validation of trichoblast-expressed dGR target genes (left) and A-type ARRs (right) after dexamethasone activation of dGR for indicated time. **B.** Phosphate response genes are similarly upregulated in wild type and *tmo5 tmo5l1* in low phosphate conditions. **C.** dGR target gene responses to low-phosphate in wild type and *tmo5 tmo5l1* double mutant backgrounds. Bars and numbers represent mean relative expression and standard error is indicated over three replicates. ns: not significant, *: p<0.05, **: p<0.01, ***:p<0.001, as determined by one-way ANOVA with post-hoc Tukey HSD testing. **D-F.** Root hair length (D), meristem length (E) and root length (F) quantifications of indicated genotypes and conditions. Lower case letters on top of boxplots indicate significantly different groups as determined by one-way ANOVA with post-hoc Tukey HSD testing (p<0.001); the number of individuals is shown at the bottom of the plot and biological repeats are indicated using different symbols.

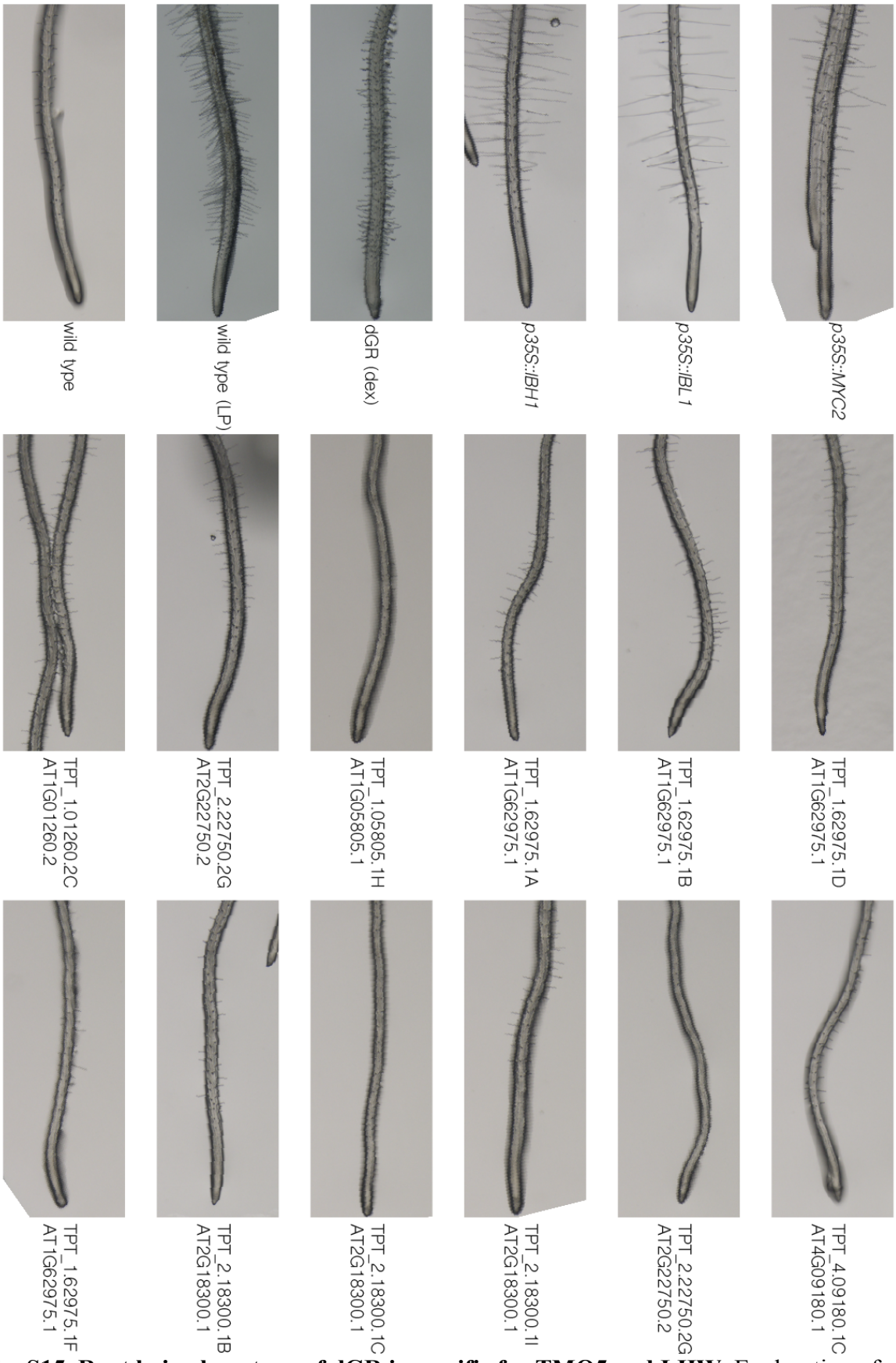

Fig. S15. Root hair phenotype of dGR is specific for TMO5 and LHW. Exploration of overexpression of several bHLH transcription factors revealed no great increase in root hairs, as compared to wild type grown on low-phosphate or dexamethasone-induced dGR.

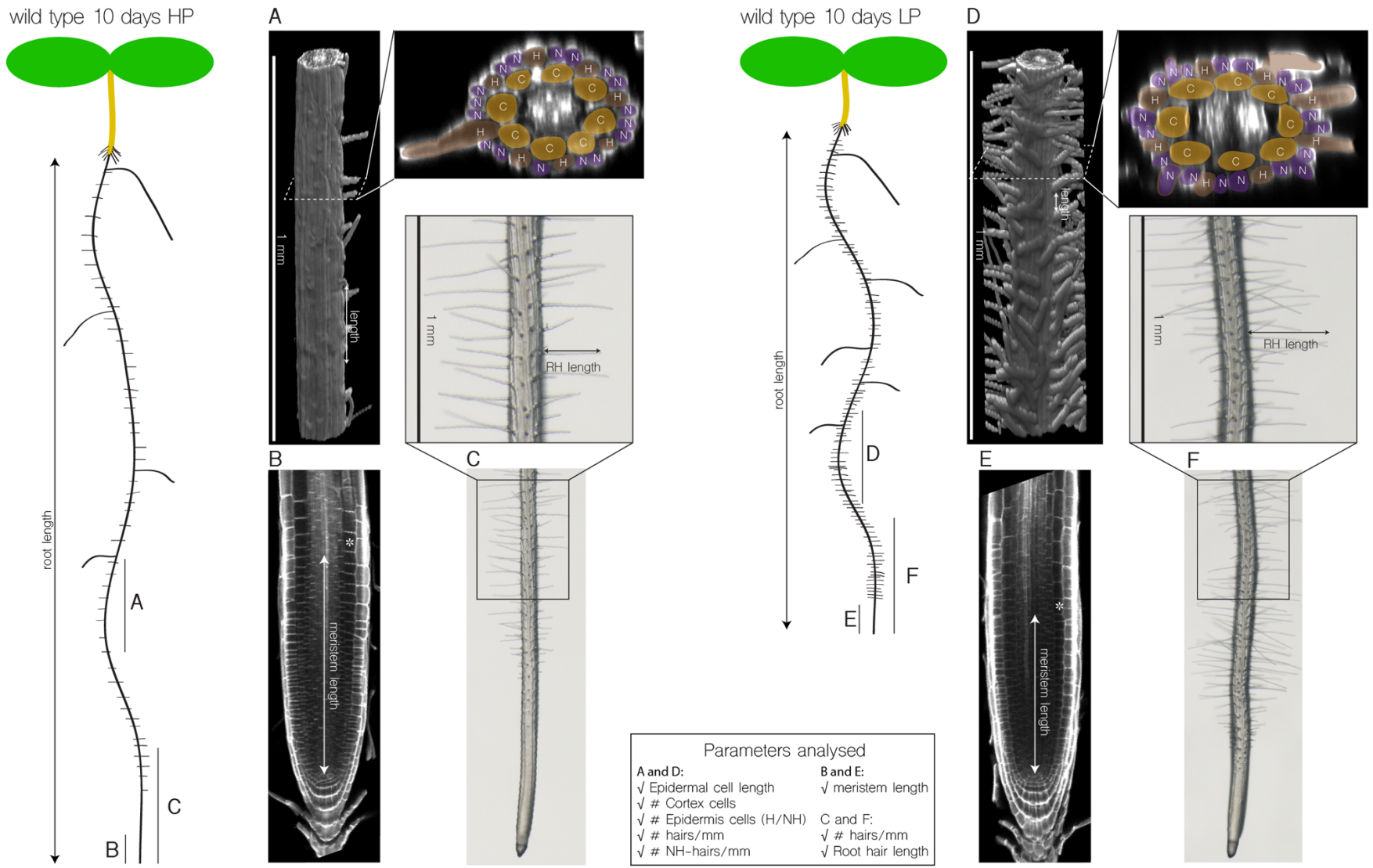

Fig. S16. Overview of the detailed phenotyping procedure. Examples and schematic overview of root hair related phenotyping and quantifications. Overview of these results is shown in **Table S2**.

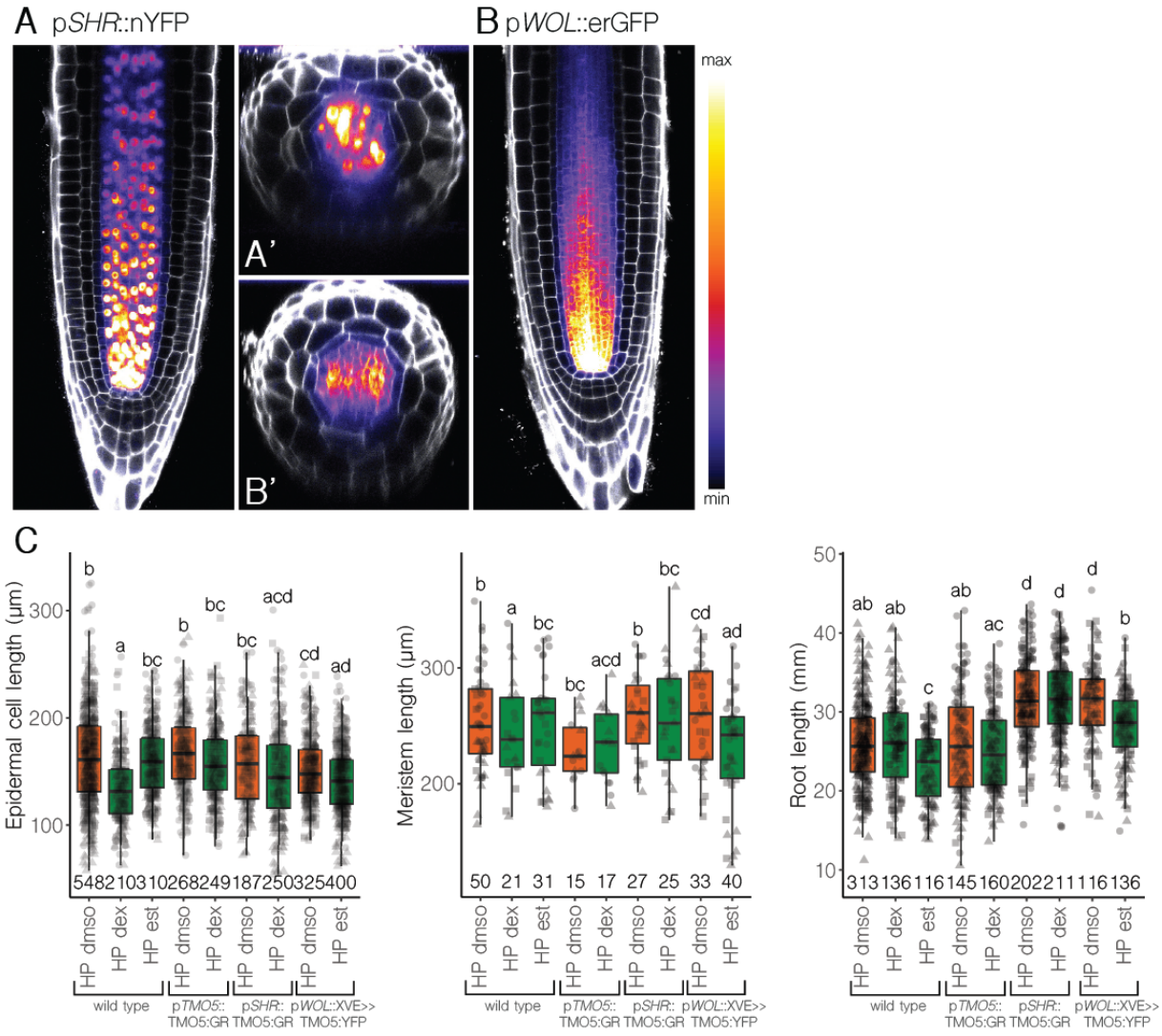

Fig. S17. A-B. Expression pattern of p*SHR*::nYFP (A) and p*WOL*::erGFP (B), showing restricted expression to the vascular domain. **C.** Epidermal cell length, meristem length and root length quantifications of indicated genotypes and conditions. Lower case letters on top of boxplots indicate significantly different groups as determined by one-way ANOVA with post-hoc Tukey HSD testing ($p<0.001$); the number of individuals is shown at the bottom of the plot and biological repeats are indicated using different symbols.

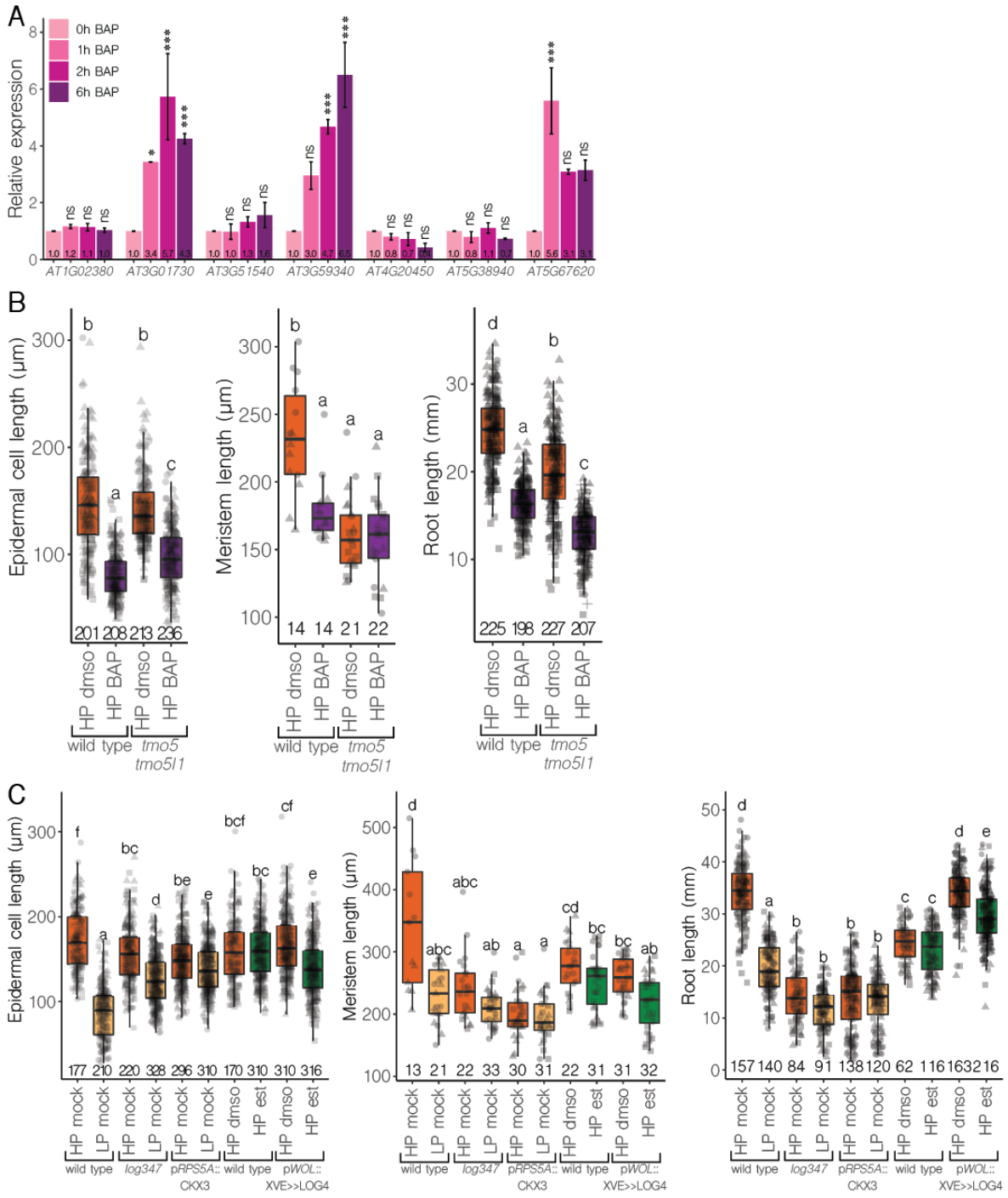

Fig. S18. A. Relative gene expression analysis using Q-RT-PCR, showing induced expression of three TMO5/LHW target genes after exogenous treatment with 10µM BAP for indicated times. Bars and numbers represent mean relative expression and standard error is indicated over six replicates in two experiments. ns: not significant, *: p<0.05, ***:p<0.001, as determined by one-way ANOVA with post-hoc Tukey HSD testing. **B-C.** Epidermal cell length, meristem length and root length quantifications of indicated genotypes and conditions. Lower case letters on top of boxplots indicate significantly different groups as determined by one-way ANOVA with post-hoc Tukey HSD testing (p<0.001); the number of individuals is shown at the bottom of the plot and biological repeats are indicated using different symbols.

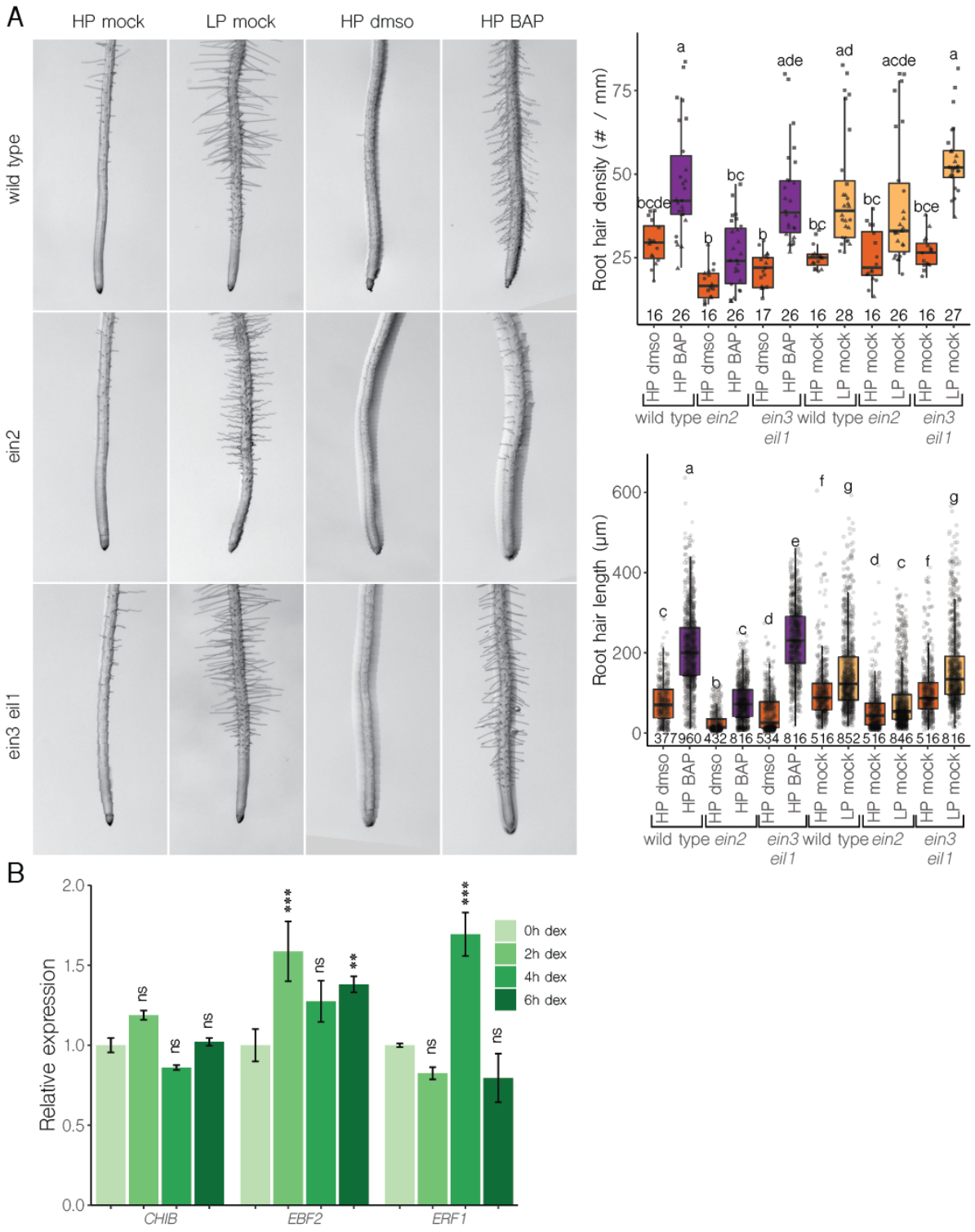

Fig. S19. A. Phenotype and quantification of root hair density and root hair length in *ein2* and *ein3 eil1* mutants grown on low phosphate and exogenous cytokinin treatment. **B.** Relative expression of three ethylene-response genes after induction of dGR as determined by Q-RT-PCR. Bars represent mean relative expression and standard error is indicated over three replicates. ns: not significant, **: p<0.01, ***:p<0.001, as determined by one-way ANOVA with post-hoc Tukey HSD testing.

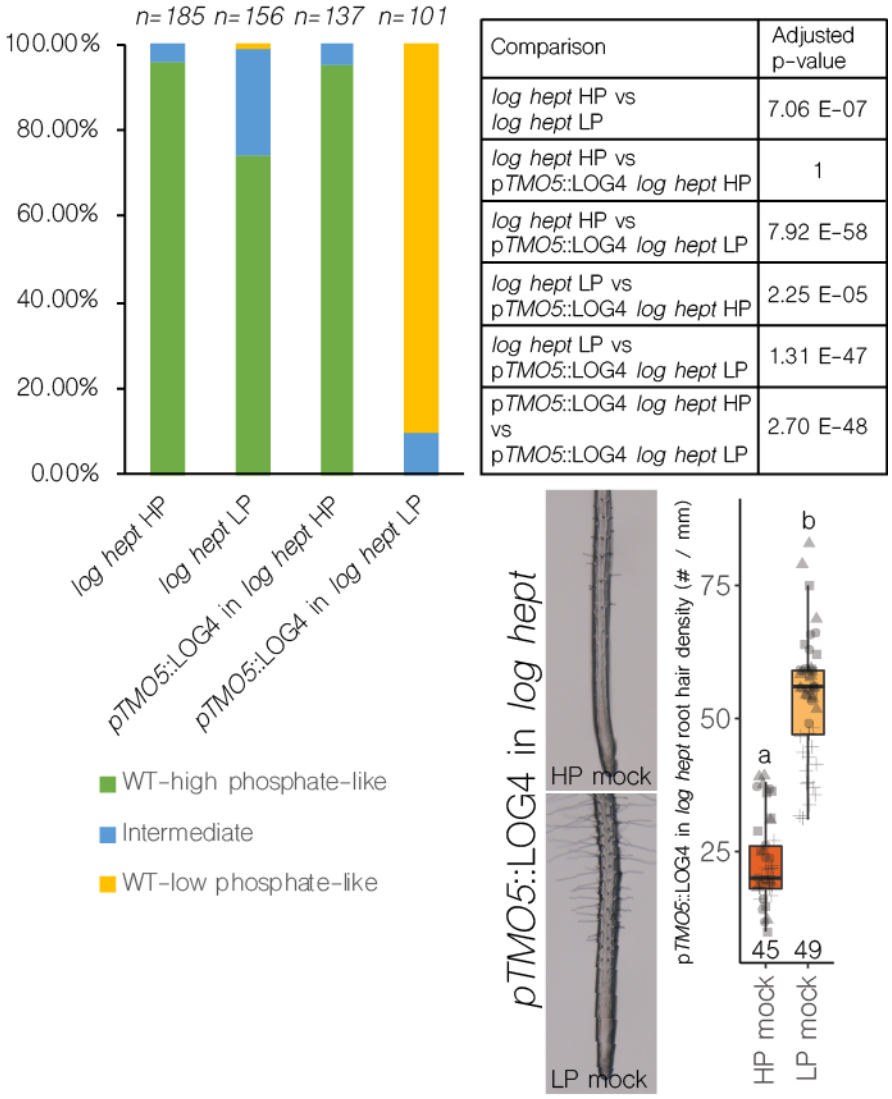

Fig. S20. Categorized phenotypic analysis of *log1234578 heptuple* mutant and *log1234578 heptuple* rescued by *TMO5* driven LOG4 (top). Table indicates adjusted p-values of the indicated comparisons as determined by Chi-square test. Phenotype and quantification of root hair density of *log1234578 heptuple* rescued by TMO5 driven LOG4. Lower case letters on top of the boxplots indicate significantly different groups as determined by one-way ANOVA with post-hoc Tukey HSD testing.

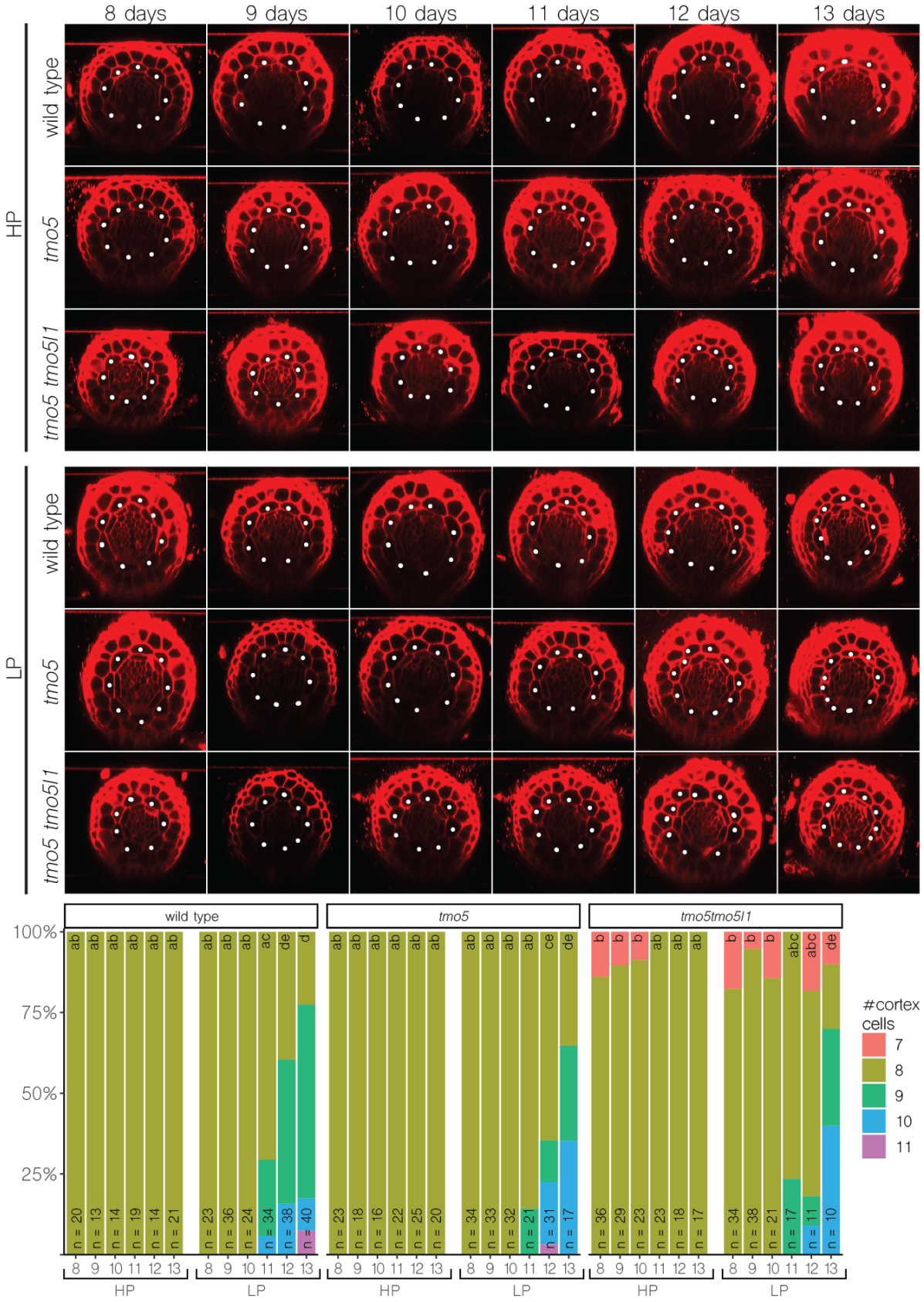

Fig. S21. Phenotype and quantification of the number of cortex cells of roots of wild type, *tmo5*, and *tmo5 tmo5l1* grown on high and low phosphate conditions for indicated number of days. Lower case letters on top of the bars indicate significantly different groups as determined by one-way ANOVA with post-hoc Tukey HSD testing ($p<0.01$).

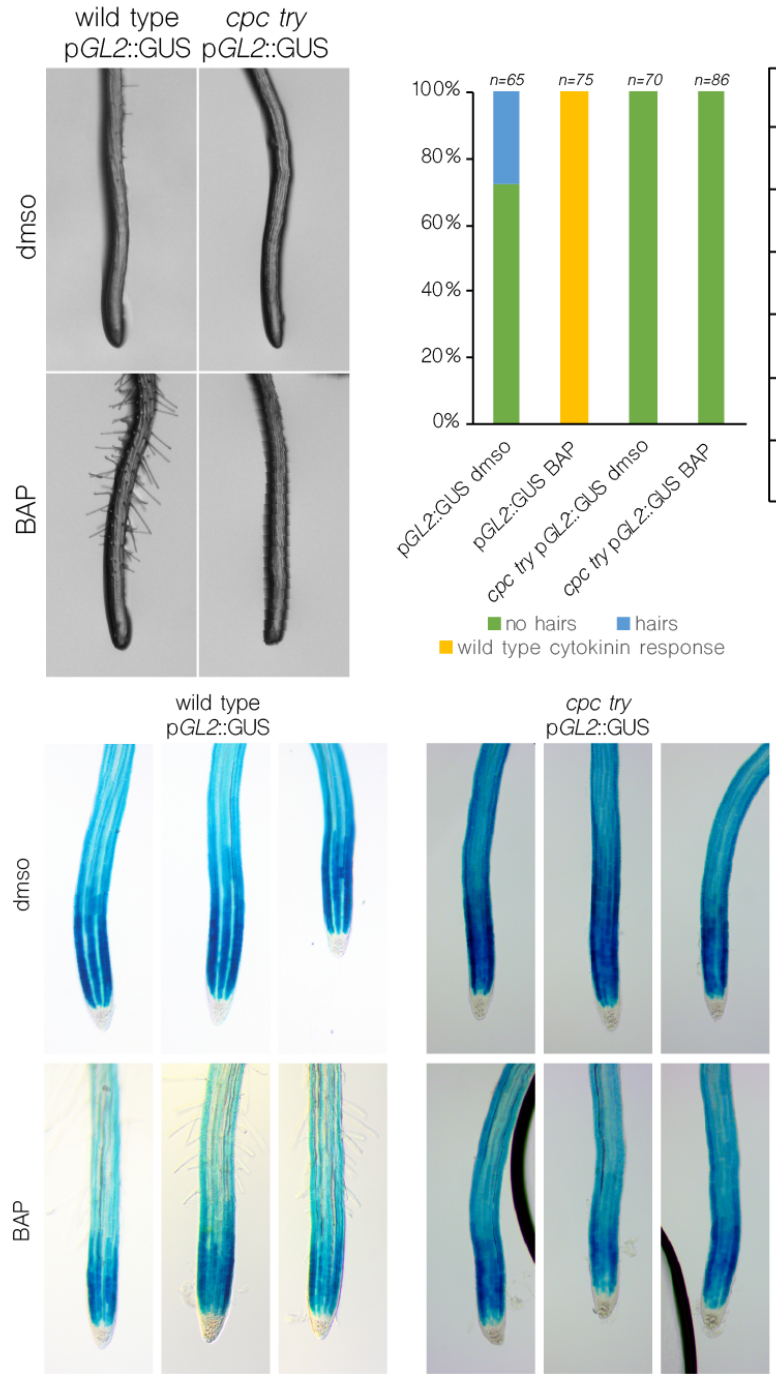

Comparison	Adjusted p-value
p*GL2*::GUS dmso vs p*GL2*::GUS BAP	2.39 E-30
p*GL2*::GUS dmso vs *cpc try* p*GL2*::GUS dmso	1.35 E-05
p*GL2*::GUS dmso vs *cpc try* p*GL2*::GUS BAP	1.20 E-06
p*GL2*::GUS BAP vs *cpc try* p*GL2*::GUS dmso	1.29 E-32
p*GL2*::GUS BAP vs *cpc try* p*GL2*::GUS BAP	4.11 E-36
cpc try p*GL2*::GUS dmso vs *cpc try* p*GL2*::GUS BAP	1

Fig. S22. Cytokinin increased root hair density is absent in *cpc try* mutants. Phenotype and quantification of wild type (Ws ecotype) or *cpc try* seedlings showing either hairs, no hairs or a wild type-like cytokinin response when grown under mock (dmso) or BAP (0.1 µM BAP in dmso) supplemented media (top) and a loss of p*GL2*::GUS absent cell files (root hair files) in the mutant and cytokinin treated wild type (bottom). Table indicates adjusted p-values of the indicated comparisons as determined by Chi-square testing.

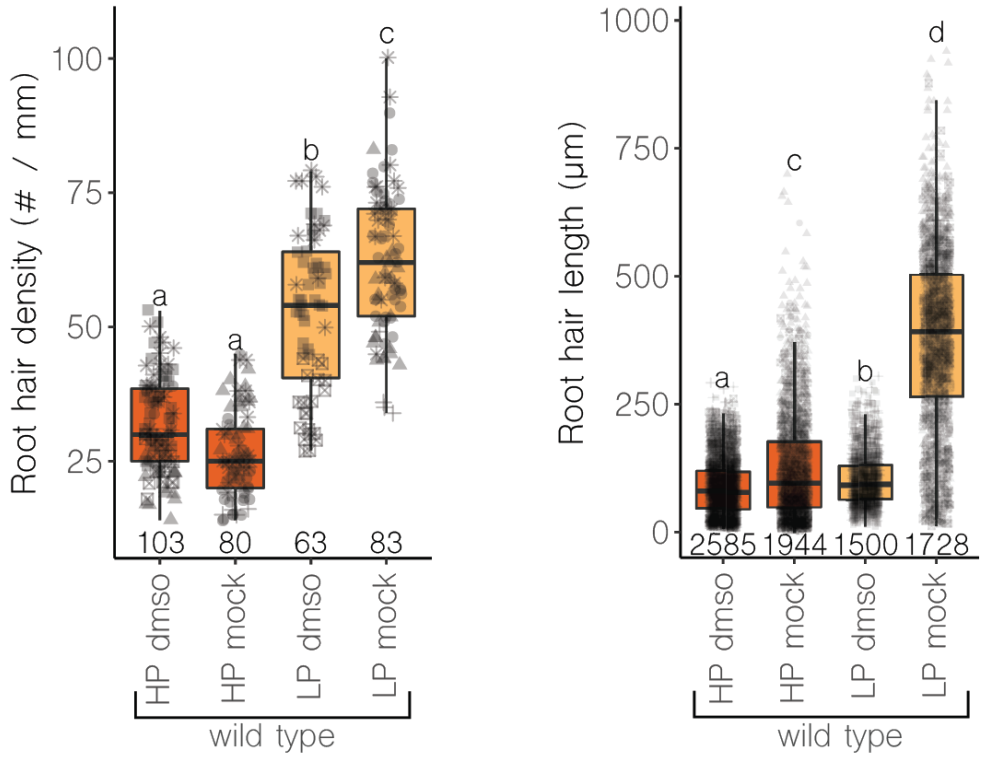

Fig. S23. Effect of solvent on root hair density and root hair length in wild type. Root hair density and epidermal cell length quantifications of wild type plants under the indicated conditions showing the dmso solvent has no effect on root hair density, but obscures the root hair length effect of low phosphate conditions. Lower case letters on top of boxplots indicate significantly different groups as determined by one-way ANOVA with post-hoc Tukey HSD testing ($p<0.001$); the number of individuals is shown at the bottom of the plot and biological repeats are indicated using different symbols.

Table S1. (separate file)

Top differential expressed genes (DEG) for each cluster (cell type) individually versus the rest of the cells.

Table S2. (separate file)

Summary of phenotyping and measurements. For each background and condition, all measured parameters are shown with number of biological repeats, total number of individuals, mean value and standard error. See Fig. S16 and materials and methods section for a more detailed description on the acquisition on these parameters.

Table S3.

Primers used in this study including gene name, AT-code, promoter length and primer sequences.

NAME	REMARK	FOR 5' – 3'	REV 5' – 3'
AT5G26260	2323 BP	GGGGACAACTTTGTATAGAAAAGTTGCATTAGTTAAGTTAACTTTTC	GGGGACTGCTTTTTTGTACAAACTTGATTTTGAGATCTTTTTTGTTTTG
AT2G43610	3020 BP	GGGGACAACTTTGTATAGAAAAGTTGGGTTTAGTTTTGGTTAAAGTTTG	GGGGACTGCTTTTTTGTACAAACTTGTTTTTTCCTTTGATGGAATGTTT
AT4G37160	3006 BP	GGGGACAACTTTGTATAGAAAAGTTGGAAATGACTGAAAAAGATAG	GGGGACTGCTTTTTTGTACAAACTTGTTTTGTAAGACGAATAGAATAT
AT1G54010	1458 BP	GGGGACAACTTTGTATAGAAAAGTTGGTGAGTTACAATTCGCCATTC	GGGGACTGCTTTTTTGTACAAACTTGTTAGAGAGTATACAGAGAGAG
AT5G55110	3009 BP	GGGGACAACTTTGTATAGAAAAGTTGCACGCATTTGGGAGAAAATAAC	GGGGACTGCTTTTTTGTACAAACTTGTTTCTCTTGATCTATGAATGTG
AT1G14220	2730 BP	GGGGACAACTTTGTATAGAAAAGTTGCCAAGATTTCTAGTAATTATAAC	GGGGACTGCTTTTTTGTACAAACTTGCTTTCTTCTCTTCTTTTCTGC
AT2G31310	1853 BP	GGGGACAACTTTGTATAGAAAAGTTGGTGAAGAAGAAGATGATAAC	GGGGACTGCTTTTTTGTACAAACTTGTCTCAAAACGTAATTATAATC
AT2G36120	3021 BP	GGGGACAACTTTGTATAGAAAAGTTGGTCTATGTTTGCTGCAAGCTC	GGGGACTGCTTTTTTGTACAAACTTGGTTTCACTCTTTCTACTTAAG
AT5G09760	2983 BP	GGGGACAACTTTGTATAGAAAAGTTGCAGCAATTGTGCTTCTTCCTC	GGGGACTGCTTTTTTGTACAAACTTGGGTTATGATTAAGAGACAG
AT2G22460	3028 BP	GGGGACAACTTTGTATAGAAAAGTTGCTTTGATACCAAATAATTTAG	GGGGACTGCTTTTTTGTACAAACTTGTGTTAATACTTCTGATGAAGC
AT4G29100	3002 BP	GGGGACAACTTTGTATAGAAAAGTTGGTTCTAAGACATGCGAGTATTC	GGGGACTGCTTTTTTGTACAAACTTGCACCTTTTATCTCTACTCTC
AT1G04240	3062 BP	GGGGACAACTTTGTATAGAAAAGTTGGTGGGATGAGTAAGAGATTTG	GGGGACTGCTTTTTTGTACAAACTTGTTCTTCAAGAATTGCAGGAG
AT1G71050	3063 BP	GGGGACAACTTTGTATAGAAAAGTTGGCTAATGATGCTTCACAAG	GGGGACTGCTTTTTTGTACAAACTTGGTCTATTACTCTCACCAAG
AT1G03010	1398 BP	GGGGACAACTTTGTATAGAAAAGTTGGCATTTTAAAAACTCAATTG	GGGGACTGCTTTTTTGTACAAACTTGCTCTCTCTATTCTCGTAGC
AT4G18780	1365 BP	GGGGACAACTTTGTATAGAAAAGTTGGTAAAGCAATTTTTTGTCATC	GGGGACTGCTTTTTTGTACAAACTTGCTTCGAATTCCCCTGTTTGG
AT2G46570	1192 BP	GGGGACAACTTTGTATAGAAAAGTTGCTGTGACCAGTGAGATCGCG	GGGGACTGCTTTTTTGTACAAACTTGCTTGAATGGAAAGAGACAAG
AT5G53730	3013 BP	GGGGACAACTTTGTATAGAAAAGTTGCTCAGTACTTTGTATTGATATC	GGGGACTGCTTTTTTGTACAAACTTGTTGGAGAGAGAGATGATGATG
AT2G43050	3007 BP	GGGGACAACTTTGTATAGAAAAGTTGCTGTCATTTCATCGGTTACG	GGGGACTGCTTTTTTGTACAAACTTGTATAGTTATGAAACTTAATG
AT4G36410	1673 BP	GGGGACAACTTTGTATAGAAAAGTTGGTAAGTTAACAACAAACAACG	GGGGACTGCTTTTTTGTACAAACTTGTTGTGTTTATTACAGTGAGTG
AT5G04080	842 BP	GGGGACAACTTTGTATAGAAAAGTTGGTAAGATATGATCTTTTGGAATTC	GGGGACTGCTTTTTTGTACAAACTTGCTTCTCAAAAGTATGGACAAAAAC
AT1G07710	2981 BP	GGGGACAACTTTGTATAGAAAAGTTGGTTTTCTTGGGAATCATTG	GGGGACTGCTTTTTTGTACAAACTTGCTTTGATACAGTCACAAAAC
AT1G07407	3043 BP	GGGGACAACTTTGTATAGAAAAGTTGGTTTTTCTAATTATCAAAAAC	GGGGACTGCTTTTTTGTACAAACTTGGGGGTTTCAGTGTCTTTAC
AT5G17450	2379 BP	GGGGACAACTTTGTATAGAAAAGTTGGTTTATTTTTTCTCAAGCATTTG	GGGGACTGCTTTTTTGTACAAACTTGTCTCTTTTTTCGTCAGCAAAAAAAC
AT5G47920	2985 BP	GGGGACAACTTTGTATAGAAAAGTTGGAGTTTACTAATTTTGTATAG	GGGGACTGCTTTTTTGTACAAACTTGATTTTTTCTTTGTAAGAGC
AT3G26290	2546 BP	GGGGACAACTTTGTATAGAAAAGTTGGATCCCGAGGAGTTTCTTCCAG	GGGGACTGCTTTTTTGTACAAACTTGTTGTATGTTATTTTGTTTTAC

AT2G29330	596 BP	GGGGACAACTTTGTATAGAAAAGTTGGTAAA ATAAAAATAACTTTTAC	GGGGACTGCTTTTTTGTACAAACTTGAGTC CTTGTATGTCAATTTTC
AT3G56220	3026 BP	GGGGACAACTTTGTATAGAAAAGTTGGATGG AATGGGTTTTATTTTTG	GGGGACTGCTTTTTTGTACAAACTTGTCTT ATATGTTTTAGCTTCTTC
AT2G40260	3018 BP	GGGGACAACTTTGTATAGAAAAGTTGCAATC AATAATGATTTTAAC	GGGGACTGCTTTTTTGTACAAACTTGCTTG GTCTCTAGCTATTTGG
AT1G16390	2040 BP	GGGGACAACTTTGTATAGAAAAGTTGCTGAG CAAAAATGATTAAAACG	GGGGACTGCTTTTTTGTACAAACTTGATAT AGGAAGAGATAGGGTTTTG
AT5G41040	2331 BP	GGGGACAACTTTGTATAGAAAAGTTGCCTCT CACGGCTGATTTGATG	GGGGACTGCTTTTTTGTACAAACTTGTTTG ATCCAAATGGAGAAAAC
AT4G16270	1384 BP	GGGGACAACTTTGTATAGAAAAGTTGCAAAA TCAAAGGTTCATAAGC	GGGGACTGCTTTTTTGTACAAACTTGTGTC GTTATATGATCACTC
AT2G40160	753 BP	GGGGACAACTTTGTATAGAAAAGTTGGTAAT AAATTTCTCCCATCC	GGGGACTGCTTTTTTGTACAAACTTGCTCG TTGTGTTCGGTTTCTG
AT1G30750	874 BP	GGGGACAACTTTGTATAGAAAAGTTGGTAAG TCTCTATCAGCTAC	GGGGACTGCTTTTTTGTACAAACTTGTTTC TTGAGTTTTCCCAGTG
AT5G46600	3039 BP	GGGGACAACTTTGTATAGAAAAGTTGGACTC CGAGGCCTCTCCGTG	GGGGACTGCTTTTTTGTACAAACTTGTTTT TTCTTTGATGTGTTCTTG
AT1G02205	1297 BP	GGGGACAACTTTGTATAGAAAAGTTGGTACA TCTTTGAATTCTTATAG	GGGGACTGCTTTTTTGTACAAACTTGTATA CCGTCGAATGTAATATG
AT4G28100	2316 BP	GGGGACAACTTTGTATAGAAAAGTTGGTAAG CCTGATCATTCACACC	GGGGACTGCTTTTTTGTACAAACTTGTCTA AATGGCTAAAGAGAGAG
AT1G17400	3012 BP	GGGGACAACTTTGTATAGAAAAGTTGGACGA TTGAGCACCTATTAAC	GGGGACTGCTTTTTTGTACAAACTTGGTTT CTTTTTTTCTGACAATTG
AT3G01840	2026 BP	GGGGACAACTTTGTATAGAAAAGTTGGTAAG GCCTCTCCTTCTATTC	GGGGACTGCTTTTTTGTACAAACTTGGTCT GACTTCTAGAGCTCC
AT3G60650	2569 BP	GGGGACAACTTTGTATAGAAAAGTTGGTACT GTCTCCTCCTCTCAATC	GGGGACTGCTTTTTTGTACAAACTTGACGA GTAGTATCGATCAAAG
AT5G48130	1662 BP	GGGGACAACTTTGTATAGAAAAGTTGCTGAA AACAAAATTAAACTTG	GGGGACTGCTTTTTTGTACAAACTTGTATT GAGTATATAAATTGTG
AT5G02070	1725 BP	GGGGACAACTTTGTATAGAAAAGTTGCTGAA ATTTAAAAACCCTTTG	GGGGACTGCTTTTTTGTACAAACTTGTTTG TTGTATAACTAATTAAG
AT3G28540	3066 BP	GGGGACAACTTTGTATAGAAAAGTTGGAGTA TATTGCAGACGCAAC	GGGGACTGCTTTTTTGTACAAACTTGCTTT GTGTTTGTTTACTTCTC
AT3G55550	3040 BP	GGGGACAACTTTGTATAGAAAAGTTGCAACA GCAAGAGCAGCCGCTTC	GGGGACTGCTTTTTTGTACAAACTTGCAAG AATTGTTTTCTTGGGAG
AT3G59340	1899 BP	GGGGACAACTTTGTATAGAAAAGTTGAGTGA AAGACGGATCGAATAAAT	GGGGACTGCTTTTTTGTACAAACTTGTATT GCAGAAGAAGCTGAGATC
AT3G01730	1220 BP	GGGGACAACTTTGTATAGAAAAGTTGGCTCA ATAACCGGGTAATCGGA	GGGGACTGCTTTTTTGTACAAACTTGTGCT ACAATATTTGATCTCC
NAME	**REMARK**	**FOR 5' – 3'**	**REV 5' – 3'**
KPNI-PTMO5-KPNI	2,9KB PROM	AAAAAAGGTACCGTGATTTTCACAATTTAAG GGTCGG	AAAAAAGGTACCTTTTTGGTTTTTTTGGTT TTTTAGTTTTTGGG
TMO5-GR FOR LIC	CDS	TAGTTGGAATGGGTTCGAAATGTACGCAATG AAAGAAGAAGAC	TTATGGAGTTGGGTTCGAACTCATTTTTGA TGAAACAGAAGC
CKX3 FOR LIC	CDS	TAGTTGGAATAGGTTCATGGCGAGTTATAAT CTTCG	AGTATGGAGTTGGGTTCCTAACTCGAGTTT ATTTTTTG
LOG4 FOR GATEWAY	CDS	GGGGACAAGTTTGTACAAAAAAGCAGGCTTT ATGGAGGTCAACAATGAAACCATGC	GGGGACCACTTTGTACAAGAAAGCTGGGT AGTCTTCAGAAGAGTAGTCAATCC
NAME	**REMARK**	**FOR 5' – 3'**	**REV 5' – 3'**
EEF	Q-RT-PCR	CTGGAGGTTTTGAGGCTGGTAT	CCAAGGGTGAAAGCAAGAAGA
UBC	Q-RT-PCR	TCCTCTTAACTGCGACTCAGG	GCGAGGCGTGTATACATTTG
ARR5	Q-RT-PCR	CCTGATTCTTTCGGCTTA	TGTATCTCTTCTCCTCTCTAA
ARR12	Q-RT-PCR	AGAGTTCGACCAGCTTCAG	ATGGAGGTCCCAGCAATG
ARR6	Q-RT-PCR	GAACATTTTGCCTCGTATTGATAG	CGAGAGTTTTACCGGCTTCA
ARR15	Q-RT-PCR	GAGAACATACAACCTCGTATAGAACAA	GCTAATTTCACCGGTTTTAGCA
AT5G38940	Q-RT-PCR	CCAACTTCAAGACTTTTGTGTCA	GGGTCCTTGCAGAACTTTCC
AT4G20450	Q-RT-PCR	AAAGAAGAAGCCATCCAAAGC	CCGCAACCTCTTCATAAGTATAGC

AT3G51540	Q-RT-PCR	AAATGGCTATCAATCACTTGGAC	CTACCACACGGTTTTCTTAGACC
AT5G67620	Q-RT-PCR	ACCAAGATGGCGCTGATAAT	ACCACCACCTCTTCCTCCA
AT3G59340	Q-RT-PCR	GCTGGTGTTGTCATGGTACTCT	TCCAGCTAGAACAAGAAAATCTCC
AT3G01730	Q-RT-PCR	GGGAACGACGAGACACTCAC	TACCAGTTGGTGACGGTGAA
AT1G02380	Q-RT-PCR	ATGATTTTGCTCCCGTTGAG	CCCGAAATTCGCTTCCTC
CHIB	Q-RT-PCR	GCCAGACTTCCCATGAAACT	CAGGGTTGTTGAGTAAGTCA
ERF1	Q-RT-PCR	GAGGATGGTTGTTCTCCGGTG	ACGGAGCGGTGATCAAAGTCA
EBF2	Q-RT-PCR	CTTTGGTTTAGGTTCGTGATAGTGC	CGAAGAGTTGTAATGGCGGATTAAG
SPX1	Q-RT-PCR	GTGTGTTTTCATTGCCGCCT	GGCTTCTTGCTCCAACAATGG
IPS1	Q-RT-PCR	CCTTTGGCAAGCTTCGGTTC	GGAGTGGGTACAACCCAAACA